A&A 462, 1051–1062 (2007)
DOI: 10.1051/0004-6361:20054505

Astronomy & Astrophysics

A method to derive the absolute composition of the Sun, the solar system, and the stars⋆

L. Piersanti[1], O. Straniero[1], and S. Cristallo[1]

INAF-Osservatorio Astronomico di Collurania Teramo, via Mentore Maggini, snc, 64100 Teramo, Italy
e-mail: [cristallo;piersanti;straniero]@oa-teramo.inaf.it

Received 10 November 2005 / Accepted 12 October 2006

ABSTRACT

Context. The knowledge of isotopic and elemental abundances of the pristine solar system material provides a fundamental test of galactic chemical evolution models, while the composition of the solar photosphere is a reference pattern to understand stellar abundances. However, spectroscopic or meteoritic abundance determinations are only possible for an incomplete sample of the 83 elements detected in the solar system. Therefore, only relative abundances are experimentally determined, with respect to H or to Si for spectroscopic or meteoritic measurements, respectively. For this reason, the available compilations of solar abundances are obtained by combining spectroscopic and meteoritic determinations, a procedure requiring the knowledge of the chemical modification occurring in the solar photosphere.

Aims. We provide a method to derive the mass fractions of the 83 elements (and their most abundant isotopes) in the early solar system material and in the present-day solar surface.

Methods. By computing a solar model, we investigate physical processes responsible for the variation of the solar surface composition in the last 4.57 Gyr. An extended network, from H to U, is coupled to our stellar evolutionary code. The effects of microscopic diffusion, rotational-induced mixing in the tachocline and radiative acceleration are discussed.

Results. The abundances of the 83 elements are given for both the pristine solar system and the solar photosphere. Calculations are repeated by adopting the most widely adopted compilations of solar abundances. Since for a given [Fe/H], the total metallicity depends on $(Z/X)_\odot$, a 30% reduction of Z is found when passing from the classical Anders & Grevesse to the most recent Lodders compilation. Some implications are discussed, such as the increase of about 700 Myr in the estimated age of Globular Clusters.

Conclusions. Within the experimental errors, the complete set of relative solar abundances, as obtained by combining meteorite and photosphere measurements, are consistent with the variations implied by the quoted physical processes. The few deviations can be easily attributed to the decay of long-lived radioactive isotopes. The large lithium depletion is only partially explained by introducing a rotation-induced mixing in the tachocline.

Key words. Sun: abundance – Sun: evolution – solar system: general – stars: abundances

1. Introduction

The Sun is the only star for which a full set of elemental abundances is available. For this reason, its composition represents the reference framework for abundance analyses in Astrophysics. In standard spectroscopic notation, abundances are given with respect to the solar composition (e.g. $[\mathrm{Fe/H}] = \log(X_{\mathrm{Fe}}/X_{\mathrm{H}}) - \log(X_{\mathrm{Fe}}/X_{\mathrm{H}})_\odot$). Then, according to a widely accepted procedure, the abundances of the various elements are obtained by *re-scaling* the solar composition: a trace element (usually iron) is used to determine the scaling factor, which is applied to all the other elements, except H and He. Thus, the distribution of heavy elements in the Sun is assumed as a sort of *cosmic* composition. Such a scenario obviously contrasts with much theoretical and observational evidence. We know that the distribution of heavy elements in the interstellar medium changes with time, as a consequence of the pollution caused by different generations of stars. The case of the enhancement of the α elements (O, Ne, Mg, Si, S, Ca, Ti) in the galactic halo, where $[\alpha/\mathrm{Fe}] \sim 0.3$–$0.6$, represents a well known example of a deviation from the scaled solar composition. A similar overabundance, also shown by the *r*-process elements, like europium, is interpreted as evidence of the fact that the early Galaxy, unlike pre-solar nebulae, was mainly polluted by massive stars. Notwithstanding these limitations, the solar composition remains an important test for models of galactic chemical evolution. Indeed, it represents a typical pattern for the evolved galactic composition, like the one shown by disk stars.

Abundances of the 83 elements found in nature have been obtained from various components of the solar system, like the Earth, Moon, planets, comets, meteorites, solar wind, solar corona and, obviously, the solar photosphere. For some elements, abundances in several solar system environments are available, whilst others can be measured just in one component. For example, heavy elements abundances are generally best measured in meteorites. On the contrary, H and other volatile elements (like C, N, O) are strongly depleted in meteorites and their abundances are typically derived from solar spectra. In some cases, as for the noble gases Ne and Ar, poor information can be found both in meteorites and in the solar photosphere, so that their abundances are derived from high energy spectra of the hot solar corona or from the solar wind. The abundances of Kr and Xe cannot be directly measured and they are usually estimated by nucleosynthesis models.

⋆ Tables 3 and 4 are only available in electronic form at http://www.aanda.org

Thus, the data set obtained from a single solar-system component is incomplete, i.e. it only includes a subsample of the 83 elements existing in the solar system. For this reason, only relative abundances[1] can be obtained (see Sect. 2). Moreover, great caution should be used when these relative abundances, as collected from different solar system environments, are combined to obtain a complete compilation. Changes with respect to the pristine composition have been produced by different physical processes (Anders & Grevesse 1989; Grevesse & Noels 1993; Grevesse & Sauval 1998; Lodders 2003; Palme & Jones 2004). For example, melting or crystallization could have produced a certain differentiation in planets and minor bodies. Among the various meteoritic phases, CI carbonaceous chondrites represent the best primitive sample of the solar system composition. On the contrary, the composition of the solar photosphere has been substantially modified since the epoch of solar system formation. Indeed, the solar surface is at the top of a deep convective region, which penetrates about 30% of the stellar radius. At the base of this region, where the temperature attains $\sim 2 \times 10^6$ K, light isotopes (e.g. D or Li) are burned via proton captures. The temperatures experienced within the convective layer of the Sun were even larger in the past 4.5 Gyr (up to $3 \div 4 \times 10^6$ K during the pre-Main Sequence). In addition, other phenomena, such as mass loss, coupled with the external convection, may have contributed to the variation of the surface composition of the Sun. Indeed, the He abundance derived from the inversion of helioseismic data ($Y_\odot = 0.2485 \pm 0.034$ – Basu & Antia 2004) can be only explained by invoking gravitational settling or, more in general, microscopic diffusion. Note that diffusion affects the whole chemical pattern. In particular, the abundances of all the isotopes more massive than $A = 12$ are depleted at the solar surface (∼–10% with respect to the original composition), whilst the mass fraction of H increases (about +5%). For this reason, photospheric abundances, usually expressed relative to H, cannot represent the original composition of the solar system. This occurrence should be carefully taken into account, especially for those elements whose abundances are almost exclusively measured in the solar photosphere (e.g. C, N, O and noble gases). Note that these elements represent about 50% of the total metallicity (Z).

In principle, a comparison between photosphere and meteorite abundances could provide direct evidence of the possible chemical modifications that occurred at the solar surface during the last 4.5 Gyr. Such a comparison reveals a general agreement between photosphere and meteorite (CI chondrites) relative abundances. In particular, according to Palme & Jones (2004), the quantity $(n(\mathrm{el})/n(\mathrm{Si}))_{\mathrm{PH}} / (n(\mathrm{el})/n(\mathrm{Si}))_{\mathrm{CI}}$[2] averaged for 34 elements with a spectroscopic uncertainty smaller than 25% is 1.004 ± 0.022 [3].

The similarity of meteoritic and photospheric relative abundances does not necessarily imply that the absolute abundances have been maintained unchanged at the solar surface. Nonetheless, this occurrence represents an important constraint to the physical processes affecting the chemical composition of the outer layer of the Sun. For instance, these processes must preserve the abundance ratios, at least within the experimental errors. The most clear deviation from this rule is represented by lithium, whose abundance relative to Si is about 2 orders of magnitude larger in meteorites than at the solar photosphere. Such a strong depletion of the photospheric Li is considered evidence for nuclear burning (mainly via p-captures) occurring at the bottom of the solar convective envelope or immediately below it (D'Antona & Mazzitelli 1984; Pinsonneault et al. 1989). Note that since p-captures rates are significantly different from one isotope to another, they represent a typical example of physical process not preserving the relative abundances.

In this paper, on the base of up-to-date Standard Solar Models (SSMs), we discuss the modifications that have occurred in the solar photosphere, since the pre-Main Sequence phase. We will show, in particular, that in SSMs where the modification of the surface composition is only caused by convective mixing and microscopic diffusion, relative abundances between heavy elements are preserved, with only a few exceptions, and, therefore, they fulfill the constraints imposed by the comparison between meteorite and photosphere relative abundances of the best measured refractory elements.

However, in many astrophysical applications and, in particular, in the calculation of stellar models, absolute, rather than relative, abundances are required, but there is no way to derive the solar absolute composition on the basis of the available measurements only. Forgetting, for a while, the differences in the chemical composition of the various solar system components and adopting a compilation obtained by combining different data sources, one may obtain a partial solution of this problem. The mass fraction of He (Y) of the present-day-solar photosphere can be independently estimated according to helioseismic measurements. Then, the detailed absolute composition of the surface layers of the present Sun can be obtained by deriving the hydrogen mass fraction (X) from the relation $X + Y + Z = Y + (1 + Z/X) \cdot X = 1$, where Z/X is known from the compilation of relative abundances. However, also in this case, the composition of the pristine solar system would remain undetermined. This problem can be solved by using a stellar evolution code to describe the past solar evolution. In this way, we are able to distinguish between present-day solar (photospheric) abundances and the composition of the pre-solar nebula. The photospheric abundances should be used to derive the composition of stars when, as usual, the results of abundance analyses are given relative to the Sun. At the same time, pristine abundances should be used to constrain the chemical evolution of the Galaxy.

Our goal is the definition of a standard procedure for the derivation of the absolute composition of the Sun and the early Solar System. We have repeated the derivation of the absolute abundances adopting the most used data sets. The main implications for various astrophysical problems requiring the knowledge of the solar composition will be discussed in Sect. 5. We do not address the largely debated question concerning the reliability of standard solar models (see for details Bahcall et al. 2004, 2005, and references therein).

2. Solar and solar system abundances

Solar (photospheric) abundances, as derived from spectroscopic analysis, are usually expressed in a logarithmic scale relative to hydrogen:

$$\varepsilon(\mathrm{el}) = \log \left[\frac{n(\mathrm{el})}{n(\mathrm{H})} \right] + 12. \quad (1)$$

In this scale the hydrogen abundance is set, by definition, to $\varepsilon(\mathrm{H}) = 12$.

[1] Hereinafter *relative abundances* indicate the abundance ratios, by mass or by number, while *absolute abundances* refer to mass or number fraction, x_i or n_i, respectively.

[2] "n(el)" is the number abundance of a generic element, while "PH" and "CI" refers to photospheric and CI carbonaceous chondrites, respectively.

[3] Here, the error of the mean has been reported.

The elemental abundances of the pristine solar system material, mainly from CI carbonaceous chondrites, are usually given relative to silicon, whose abundance is fixed to 10^6 atoms:

$$N(\mathrm{el}) = \frac{n(\mathrm{el})}{n(\mathrm{Si})} \times 10^6. \quad (2)$$

The solar and the solar system abundance scales are to refer as *astronomical* and *cosmochemical* scales, respectively. As recalled in the Introduction, they are both incomplete, so that the available compilations of solar chemical abundances necessarily contain data from different sources. Following a commonly adopted procedure, the meteoritic abundances are "translated" from the cosmochemical into the astronomical scale by means of the following relation:

$$\varepsilon(\mathrm{el}) = R + \log\left(N(\mathrm{el})\right). \quad (3)$$

Here the re-scaling factor R is obtained by inverting Eq. (3) for silicon, whose abundances in the cosmochemical and in the astronomical scales are firmly measured (Lodders 2003), or by taking an average value over a selection of few elements detectable both in meteorites and in the solar photosphere (e.g. Cameron 1973, 1982; Grevesse 1984; Anders & Grevesse 1989; Palme & Beer 1993). Such a procedure was first proposed by Suess & Urey (1956), according to the pioneering work of Clarke (1889), and it was based on the implicit assumption of the existence of a unique cosmochemical pattern. We know that this statement is not correct. However, the re-mapping procedure remains correct, provided that the evolution of the surface composition of the Sun preserves the relative abundance ratios. In this case, by summing and subtracting $\log\left(n(\mathrm{Si}) \times 10^6\right)$ from the right side of Eq. (1), one obtains:

$$\varepsilon(\mathrm{el}) = \log\left[\frac{n(\mathrm{el})}{n(\mathrm{Si})} \times 10^6\right] + \log\left[\frac{n(\mathrm{Si})}{n(\mathrm{H})} \times 10^{-6}\right] + 12. \quad (4)$$

Then, by using the definition of $N(\mathrm{el})$ in Eq. (2) and putting $R = \log\left[\frac{n(\mathrm{Si})}{n(\mathrm{H})}\right] + 6$, we can recognize that the last equation coincides with Eq. (3). Therefore, if the evolution of the Sun preserves the ratios $n(\mathrm{el})/n(\mathrm{Si})$, the same (photospheric) abundance $\varepsilon(\mathrm{el})$ can be obtained by using the definition in Eq. (1) or in Eq. (3).

The most frequent misunderstanding in the practical use of the abundance compilations obtained by combining photosphere and meteorite data concerns the comparison between the values of $\varepsilon(\mathrm{el})$ obtained from spectroscopy (astronomical scale, as defined by Eq. (1)) and those obtained by re-mapping the cosmochemical into the astronomical scale according to Eq. (3). The similarity of the two scales is often interpreted as a problem for SSMs including microscopic diffusion, because they imply a depletion of the heavy elements at the solar photosphere (see e.g. Grevesse & Sauval 1998). Such a conclusion has been questioned by Lodders (2003) by the observation that microscopic diffusion could have affected by the same amount the abundances of heavy elements, so that the relative ratios would be preserved. In the following, we will demonstrate that this is the case.

If the isotopic, rather than the elemental, composition is needed, further difficulties should be considered. In some cases, precise isotopic ratios can be obtained for meteorites, but their spectroscopic determination is limited by the small isotopic shift of the atomic lines relative to their width. For this reason, the standard procedure makes use of the very precise terrestrial values, as provided by the IUPAC facility, although they are representative of "the chemical materials encountered in the laboratory" not necessarily of "the most abundant natural material" (Anders & Grevesse 1989; see also Lodders 2003).

3. Standard solar model

In order to investigate the change of the solar surface composition induced by different physical processes and to derive the absolute compositions of the solar photosphere and of the solar system, we make use of a Standard Solar Model. We have simulated the evolution of the Sun, from the pre-Main Sequence to the present day, by using the FRANEC evolutionary code (Chieffi et al. 1998).

3.1. Input physics

An extended nuclear network, including all the elements from H to U, has been adopted. For each element, the evolution of all stable and some long-lived isotopes have been explicitly followed (286 isotopes in all). Reaction rates of relevant strong interactions are generally taken from the NACRE compilation (Angulo et al. 1999) with a few important exceptions. The $^{14}\mathrm{N}(\mathrm{p},\gamma)^{16}\mathrm{O}$ rate is computed according to Imbriani et al. (2005), while the $\mathrm{D}(\mathrm{p},\gamma)^3\mathrm{He}$ is derived from Casella et al. (2002). β-decay rates are taken from Oda et al. (1994) for $T > 10^7$ K, while for lower temperature the terrestrial values are assumed. The only exception is the β^+ rate of $^{26}\mathrm{Al} \rightarrow {}^{26}\mathrm{Mg}$, which is derived from Coc et al. (2000). The cross section for the e-capture on ^{7}Be has been derived from Caughlan & Fowler (1988).

Electron screenings are evaluated according to Dewitt et al. (1973) and Graboske et al. (1973), for the weak and intermediate regimes, and to Itoh et al. (1977) and Itoh et al. (1979), for the strong one.

Microscopic diffusion of each isotopes is taken into account by inverting the coupled set of Burgers equations (Thoul et al. 1994). In the evaluation of the Coulomb logarithm, full ionization has been assumed. This approach, which may be considered as "standard" in the computation of SSMs (see Bahcall et al. 2004, and references therein), presents some limitations. The ionization degree of the various species should be taken into account when computing the diffusion coefficients in the most external layers of the star. In practice, the greater the ionization, the larger the Coulomb cross section and, in turn, the smaller the diffusion coefficient. Since the Sun presents a rather deep external convective envelope, the degree of ionization of the various chemical species should be carefully evaluated at the bottom of this zone. Another process often neglected is the acceleration caused by the net transfer of momentum from the outcoming photon flux to nuclei and electrons. This process acts opposite to the gravitational settling on heavy elements. The effect of all these processes on SSMs have been studied by Turcotte et al. (1998). They computed the fraction of momentum transported by radiation that is absorbed by the different chemical species. They also took into account the partial ionization in the computation of diffusion coefficients. According to their results, the radiative acceleration largely compensates the increase of the diffusion efficiency due to partial ionization of the various isotopes. The combined effect of these two processes is a variation of the average diffusion efficiency of about 10% with respect the one obtained by neglecting the radiative acceleration and assuming fully ionized matter. Turcotte and co-workers also showed that the Rosseland mean opacity calculated by interpolating on tables of various Z, but the same heavy element distribution, cannot be distinguished from that computed by taking into account the variation of the relative abundances due to all these processes. Considering the results of Turcotte et al. (1998), in the present work we do not account for these "non-standard" effects, even if a more precise evaluation of the absolute solar composition

would require their proper inclusion in the computation of SSMs. In particular, since the degree of ionization changes from one nucleus to another, it should be carefully verified that these processes, whose efficiency depends on the effective charge, do not alter the abundance ratios of the 34 elements for which a very good agreement between the astronomical and the cosmochemical scales have been found. We will further comment on this point in Sect. 4.1.

The borders of the convective unstable zones have been evaluated by means of the Schwartzschildt criterion. In these layers, the temperature gradient is calculated by means of the mixing length theory (Cox & Giuli 1968). As usual, the ratio of the mixing length and the pressure scale height is one of the three free parameters of the SSM (see the next section).

The equation of state (EOS) for $T > 10^6$ K is an improved version of the one described by Straniero (1988) (see Prada Moroni & Straniero 2002). At lower temperature, a Saha equation has been used to derive the population of the various ionization states and of the fractions of H molecules (H_2 and H^-). More accurate equations of state, such as the OPAL (Rogers et al. 1996) and the MHD (Mihalas et al. 1990, and references therein), may provide a better description of the thermodynamical quantities needed to calculate a SSM, but they do not cover the full range of temperature and density experienced by the core of off-Main Sequence stars. For this reason we prefer our EOS to those commonly adopted by the solar community. A comparison of the SSM computed with our EOS and the one obtained by adopting the OPAL EOS is discussed in the next section.

We have repeated the calculation of the SSM by changing the adopted compilation of relative solar abundances, namely:

1. **AG89**: Anders & Grevesse (1989);
2. **GN93**: Grevesse & Noels (1993);
3. **GS98**: Grevesse & Sauval (1998);
4. **Lo03**: Lodders (2003).

The main differences among these compilations concern the abundances of carbon, nitrogen, oxygen, neon and argon. We choose these four compilations because they are considered fundamental steps toward our comprehension of the cosmic composition. The AG89 mixture is a complete and systematic analysis of chemical abundances of the various solar system components and it is widely considered the reference framework for studies of chemical evolution of the Galaxy. The GN93 compilation has been extensively used in the past to compute stellar models (Straniero et al. 1997; Bono et al. 1997; Salaris et al. 1997; Pols et al. 1998; Girardi & Bertelli 1998; Dominguez et al. 1999; Charbonnel et al. 1999; Bono et al. 2000; Maeder & Meynet 2001), mainly because the opacity tables provided by the OPAL group (Rogers & Iglesias 1992; Iglesias & Rogers 1996) were originally computed assuming this distribution of heavy elements. The GS98 compilation represents the last upgrade of the series started by Anders & Grevesse (1989) and it has been adopted in computing the most recent large database of stellar evolutionary tracks and isochrones (e.g. Kim et al. 2002; Pietrinferni et al. 2004). The Lo03 distribution of heavy elements is representative of the most recent analysis of carbon, nitrogen, oxygen, neon and argon abundances as derived by 3D-atmospheric models (Asplund et al. 2000, 2004; Asplund 2000; Allende Prieto et al. 2001, 2002).

For each set of solar abundances, tables of radiative opacity have been derived through the web facility provided by the OPAL group (`http://www-phys.llnl.gov/Research/OPAL/opal.html`). These opacity tables extend down to $\log T = 3.75$ and are suitable for the calculation of Main Sequence models of a 1 $M_\odot$ star. However, additional low temperature opacities are needed to calculate the cooler pre-Main Sequence models. In this case, we use the tables provided by Alexander & Ferguson (1994) for a fixed composition (GN93). Since the use of these low temperature opacities is limited to pre-Main Sequence models, it does not significantly affect our prediction concerning the composition of the present Sun. The opacity change caused by the variation of the internal chemical composition, as due to nuclear burning, convective mixing and microscopic diffusion, has been taken into account by interpolating between tables with different Z and Y (for a description of the numerical procedure adopted to interpolate opacity tables see the next subsection).

3.2. SSM check

For each set of relative abundances, we vary the initial metallicity ($Z_{\rm in}$), the helium mass fraction ($Y_{\rm in}$) and the value of the α parameter (the ratio between mixing length and pressure scale height), until the best reproduction of the present-day values of the solar radius ($R_\odot$), luminosity ($L_\odot$) and $(Z/X)_\odot$ is obtained. The initial composition (n_i, i = 1, ..., 83) is calculated by inverting Eq. (1), where $n({\rm H}) = (1 - Y_{\rm in} - Z_{\rm in})$, while ε(el) are taken from one of the adopted compilations of relative abundances.

For the solar luminosity, radius, mass and age we adopt $L_\odot = 3.844 \times 10^{33}$ erg s^{-1}, $R_\odot = 6.951 \times 10^{10}$ cm, $M_\odot = 1.989 \times 10^{33}$ g and $t = 4.57 \times 10^9$ yr, respectively. $(Z/X)_\odot$ is obviously different for the four set of solar relative abundances, namely: 0.02668 (AG89), 0.02439 (GN93), 0.02292 (GS98) and 0.01763 (Lo03). The mass is maintained constant.

In order to investigate the reliability of our input physics we have performed several calculations by varying both the interpolation on the tables of opacity coefficients and the equation of state and comparing the resulting sound-speed profile with that inferred from the GOLF+MDI data (Lazrek et al. 1997; Kosovichev et al. 1997).

The best interpolation method cannot be easily fixed according to mathematical or physical arguments. Then, we have directly evaluated the influence of this interpolation on the SSM. The different numerical schemes we have considered are listed below:

- K0: cubic interpolation of κ in $R = \rho \times 10^{12}/T^3$, T and Y and linear interpolation in Z;
- K1: OPACGN93.F routine provided by the OPAL group. Such a routine performs an "interpolation between overlapping quadratics" in order to obtain a smoothed opacity;
- K2: cubic interpolation of $\log(\kappa)$ in $\log(R)$ and T and a linear interpolation of κ in Y and Z;
- K3: cubic interpolation of $\log(\kappa)$ in R, T and Y and a linear interpolation of κ in Z.

The results are summarized in Fig. 1, where we report the difference in the sound-speed inferred from the GOLF+MDI data (Lazrek et al. 1997; Kosovichev et al. 1997) and the various test models. In Table 1 we list some relevant quantities for the same models in Fig. 1. All these SSM were computed by using the GN93 compilation of solar abundances. The position of the inner border of the solar convective envelope changes when changing the interpolation scheme. For the particular set of SSM in Table 1, the variation of $R_{\rm CE}$ is one order of magnitude larger than the statistical error of the helioseismic data ($\Delta R_{\rm CE} = 0.001\, R_\odot$ – see Basu & Antia 2004, and references therein). The run of the sound speed is particularly sensitive to

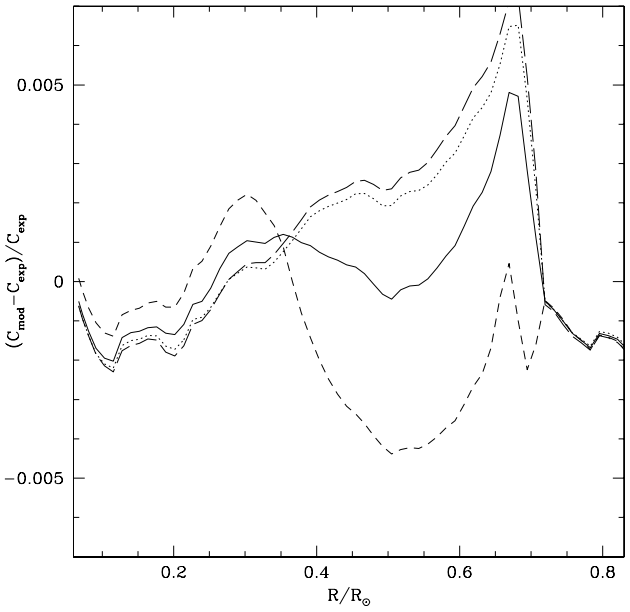

Fig. 1. Sound-speed difference between GOLF+MDI data ($C_{\rm exp}$) and various theoretical models ($C_{\rm mod}$): K0 (*solid line*), K1 (*long-dashed line*), K2 (*dotted line*), K3 (*dashed line*). For details see text.

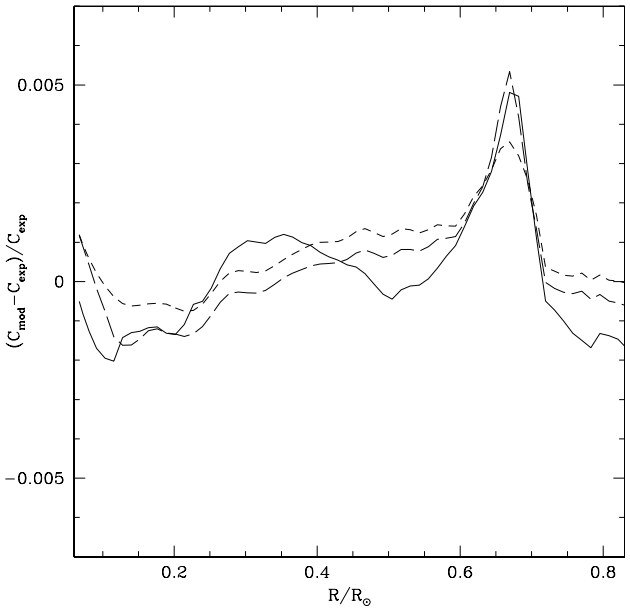

Fig. 2. Sound-speed difference between GOLF+MDI data ($C_{\rm exp}$) and two models ($C_{\rm mod}$) obtained by adopting different equation of state: our EOS (*solid line*) and EOS_2005 (*long-dashed line*). The dashed line refers to the SSM of Bahcall et al. (1998).

Table 1. Selected quantities for SSMs obtained by adopting various interpolation schemes for the calculation of opacity coefficients (models from K0 to K3) and by using the most recent OPAL EOS (EOS_2005): the value of the radius at the base of the convective envelope ($R_{\rm CE}$), the mass extension of the convective envelope ($\Delta M_{\rm CE}$), the value of the mixing length parameter α, the photospheric mass fraction abundance of hydrogen (X), helium (Y) and metallicity (Z) and their initial values.

	K0	K1	K2	K3	EOS_2005
$R_{\rm CE}/R_\odot$	0.71420	0.71755	0.71670	0.70523	0.71431
$\Delta M_{\rm CE}/M_\odot$	0.02371	0.02257	0.02284	0.02647	0.02376
α	2.25935	2.26263	2.27479	2.36326	1.86171
$X_\odot$	0.73528	0.73730	0.73751	0.72935	0.73835
$Y_\odot$	0.24678	0.24472	0.24450	0.25286	0.24365
$Z_\odot$	0.01793	0.01798	0.01799	0.01779	0.01801
$X_{\rm in}$	0.70713	0.70322	0.70361	0.69669	0.70581
$Y_{\rm in}$	0.27834	0.27675	0.27636	0.28363	0.27421
$Z_{\rm in}$	0.01994	0.02003	0.02003	0.01968	0.01998

the adopted opacity interpolation in the intermediate region, up to the base of the convective envelope ($0.3 \leq R/R_\odot \leq 0.72$). In the following we will adopt the K0 interpolation scheme.

To check the reliability of the adopted EOS, we have computed an additional SSM by using the K0 interpolation and the OPAL EOS_2005 (`http://www-phys.llnl.gov/Research/OPAL/EOS_2005/`). The original routine provided by OPAL has been used to interpolate data in the EOS tables. The sound speed difference between the experimental data and this SSM is shown in Fig. 2. In the same figure, we also report the same quantity for the K0 model of Fig. 1 and for the SSM by Bahcall et al. (1998). All the 3 models provide a good reproduction of the measured sound speed, the deviation being confined within ±0.002, with the exception of the well known discrepancy at the base of the external convective zone. As expected, in the most external zone, the EOS_2005 provides a better evaluation of the thermodynamical quantities than the Saha equation. Note that the SSMs computed with the Saha EOS require a rather large value of α, i.e. the mixing length parameter. As a whole, the model obtained with our EOS (K0) provides a reasonable reproduction of the present Sun, at least comparable to the one obtained with the OPAL EOS (see Table 1).

In Table 2 we summarize the main features of the SSMs computed by adopting the four compilations of solar abundances described in the previous section. The most important difference is the variation of the initial (pre-solar) metallicity ($Z_{\rm in}$), which decreases from $Z = 0.02177$ (AG89) to 0.01487 (Lo03). The most recent compilation of solar abundances also implies a lower initial abundance of He ($Y_{\rm in}$ in Table 2), namely $Y_{\rm in} = 0.2776$ (AG89) and 0.2674 (Lo03).

The simultaneous reduction of $Z_{\rm in}$ and $Y_{\rm in}$ leaves the ratio $\Delta Y/\Delta Z$ almost unchanged. Indeed, by taking $Y = 0.245$ for the cosmological He (Spergel et al. 2003), one gets $\Delta Y/\Delta Z \sim 1.5$ for both AG89 and Lo03. This value is definitely lower than that derived from H II regions and planetary nebulae (see Esteban & Peimbert 1995).

Nevertheless, these differences in Z and Y affect the opacity and, in turn, the internal temperature profile and the stellar radius. In this context, the reduction of the metallicity is partially counterbalanced by the reduction of the He content. The combined effect is a net reduction of the opacity, when passing from AG89 to Lo03. This reduction is about 7% near the base of the convective envelope (Bahcall et al. 2004). As a consequence, the external convective zone shrinks (see $R_{\rm CE}$ in Table 2). Note that in the Lo03 model, the location of the inner border of the convective envelope is definitely larger than the one derived from the observed frequencies of solar oscillations, namely $R_{\rm CE} = 0.7295$ to be compared with 0.713 ± 0.001 (Basu & Antia 1997). In addition, a lower α is required to reproduce the observed solar radius. This occurrence may affect the properties of stellar models that, as usual, adopt a solar calibrated mixing length parameter. We will briefly discuss this point in the final section.

Table 2. Selected quantities for our best SSMs computed by adopting different abundance compilations: the value of the radius at the base of the convective envelope (R_{CE}), the mass extension of the convective envelope (ΔM_{CE}), the temperature (T_{CE}) and density (ρ_{CE}) at the base of the convective envelope, the value of the mixing length parameter α, the central value of temperature (T_c) and density (ρ_c), hydrogen (X_c) and helium (Y_c) abundances at the center (by mass fraction), the current-age photospheric (Z/X), X, Y and Z and their initial values (see text).

	AG89	GN93	GS98	Lo03
$R_{CE}/R_\odot$	0.71110	0.71426	0.71621	0.72949
$\Delta M_{CE}/M_\odot$	0.02459	0.02367	0.02316	0.01940
T_{CE} (in 10^6 K)	2.22662	2.18691	2.16374	2.01571
ρ_{CE} (in g cm^{-3})	0.19015	0.18349	0.17983	0.15255
α	2.27016	2.25772	2.25112	2.14243
T_c (in 10^6 K)	15.7591	15.7065	15.6846	15.5818
ρ_c (in g cm^{-3})	155.008	154.380	154.169	152.714
X_c	0.32948	0.33419	0.33636	0.34680
Y_c	0.64675	0.76554	0.64297	0.63698
$(Z/X)_\odot$	0.02669	0.02439	0.02292	0.01762
$X_\odot$	0.73103	0.73542	0.73757	0.74792
$Y_\odot$	0.24940	0.24664	0.24553	0.23890
$Z_\odot$	0.01951	0.01793	0.01690	0.01381
$(Z/X)_{in}$	0.03107	0.02841	0.02673	0.02074
X_{in}	0.69732	0.70175	0.70383	0.71267
Y_{in}	0.28102	0.27831	0.27736	0.27256
Z_{in}	0.02166	0.01994	0.01881	0.01478

4. Proto-solar vs. solar abundances

In this section we illustrate the procedure followed to evaluate the mass fractions of isotopes and elements at the photosphere of the present Sun as well as in the early-solar-system material.

First of all let us assume that:

$$\left(\frac{n_k}{n_j}\right)_\odot = \left(\frac{n_k}{n_j}\right)_{CI} \qquad j,k = 3,\ldots,83 \tag{5}$$

where the suffixes "$\odot$" and "CI" refer to the solar photosphere and the pristine material (CI carbonaceous chondrites), respectively. This is a generalization of the assumption already made to translate the cosmochemical into the astronomical scale (see Eq. (3), where $j = 14$, the Si atomic number). Equation (5) has been proved for most of the elements whose abundances can be derived from both meteorites and the solar photosphere, with the exception of lithium. However, since the Li abundance is small compared to the total metallicity, its deviation from this general rule does not affect our estimation of the absolute abundances of other elements. Thus, we extend the validity of Eq. (5) to all the elements, H and He excluded.

Since $(x_k/x_j) = (n_k/n_j)\cdot(A_k/A_j)$ [4], the previous relation can be re-written as:

$$\left(\frac{x_k}{x_j}\right)_\odot = \left(\frac{x_k}{x_j}\right)_{CI}. \tag{6}$$

Here we are assuming that the isotopic ratios remain (almost) unchanged over the solar system lifetime, so that $\left(\frac{A_k}{A_j}\right)_\odot = \left(\frac{A_k}{A_j}\right)_{CI}$. For a few elements with radioactive isotopes whose decay time is comparable to the solar age (see next section), this assumption is not correct. Also in this case, since their abundances are small compared to the total metallicity and their impact on the SSM is negligible, we can correct their early solar system abundances, without affecting the evaluation of the abundances of the other elements. Then, by summing over the index k, we obtain Z/x_j [5] and dividing Eq. (6) by this quantity, it follows that:

$$\left(\frac{x_k}{Z}\right)_\odot = \left(\frac{x_k}{Z}\right)_{CI} \qquad k = 3,\ldots,83. \tag{7}$$

In other words, the mass fraction of a given element in the solar photosphere and the corresponding one in the early solar system material scale as the ratio $Z_\odot/Z_{in}$. Hence, we can invert Eq. (1) to find the following set of equations:

$$\frac{x_k}{X} = 10^{\varepsilon(k)-12}\frac{A_k}{A_H} \qquad k = 3,\ldots,83 \tag{8}$$

where X is the hydrogen mass fraction. If X would be known, the mass fractions of all the elements could be derived from these equations, but, unfortunately, it cannot be directly measured at the solar photosphere. Since we have used the astronomical scale, this equation can only be applied to the photospheric abundances. A more general relation, valid for any scaled solar composition, can be determined by summing all the Eqs. (8), thus obtaining:

$$\left(\frac{Z}{X}\right)_\odot = \sum_{k=3}^{83} 10^{\varepsilon(k)-12}\frac{A_k}{A_H}. \tag{9}$$

Then, dividing Eqs. (8) by (9) we find:

$$\frac{x_k}{Z} = \frac{10^{\varepsilon(k)-12}\frac{A_k}{A_H}}{\sum_{j=3}^{83} 10^{\varepsilon(j)-12}\frac{A_j}{A_H}} = 10^{\varepsilon(k)-12}\frac{A_k}{A_H}\left(\frac{Z}{X}\right)_\odot^{-1} \quad k = 3,\ldots,83. \tag{10}$$

Remembering our basic assumption, as expressed in Eq. (7), this formula can be used to calculate the early solar system composition, once the value of Z_{in} is known. The same formula can be used to derive the absolute abundances of any star having a scaled-solar composition, once its metallicity (Z) is given.

In practice, we start with a tentative set of Z_{in}, Y_{in} and α. Then, with Eqs. (10) and by taking terrestrial ratios among isotopes of the same element (but applying appropriate corrections to the radioactive isotopes), we calculate the initial mass fraction of all the 286 isotopes and we compute a first evolutionary sequence up to the solar age. Then, the initial values of Z, Y and α are corrected and the procedure is iterated, until a good reproduction of $R_\odot$, $L_\odot$ and $(Z/X)_\odot$ is simultaneously obtained[6]. Note that, for the initial composition, we generally choose meteoritic (CI) relative abundances, if available. For this reason, we obtain $(Z/X)_\odot$ values that are slightly different to those quoted in the original papers reporting the four solar abundance compilations, where somewhat different choices are adopted.

In Table 3 we list the isotopic composition (initial and present-day) for the four SSMs, with the the corresponding depletion efficiency $\delta = 100\cdot(1 - X_\odot/X_{in})$. In Table 4 we report, for the four SSMs, the initial mass fraction, the present-day mass fraction, the ratio $P = (n(\mathrm{el})/n(\mathrm{Si}))_{in}/(n(\mathrm{el})/n(\mathrm{Si}))_\odot$ and the R parameter. Now, we can check the consistency of our basic assumption, that is: the evolution of the solar surface composition has occurred preserving the abundance ratios of heavy elements.

[4] x_j is the mass fraction of the jth element and A_j is the corresponding average atomic mass. For each element, this average can be calculated by means of the terrestrial isotopic ratios provided by IUPAC.

[5] Here Z represents the total metallicity.

[6] We stop the iterations when $\delta R/R_\odot$, $\delta L/L_\odot$ and $\delta(Z/X)/(Z/X)_\odot$ become smaller then 10^{-5}.

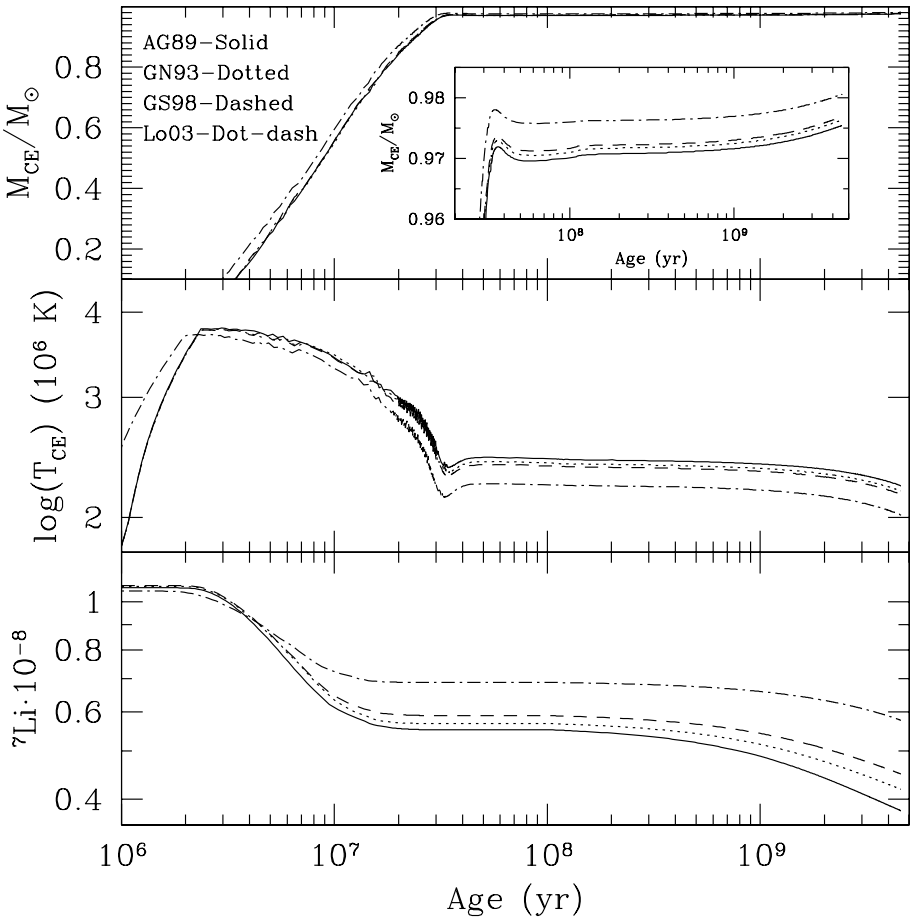

Fig. 3. Evolution of: mass coordinate (in solar unit) of the inner border of the convective envelope (*upper panel*); temperature at the base of the convective envelope (*middle panel*); lithium abundance by mass fraction (*lower panel*).

4.1. $Z \geq 6$

Owing to the rather fast mixing induced by convection, the composition within the most external 30% of the solar radius is maintained homogeneous. Thus, the photospheric composition changes mainly due to processes occurring at the base of the convective envelope. Elements with $Z \geq 6$ are not affected by nuclear burning, because the temperature within this convective layer never exceeds a few million K (see the middle panel in Fig. 3), not enough for *p*-capture to occur on these elements. As a consequence, the variation of their surface abundances is only determined by microscopic diffusion occurring at the base of the convective envelope.

We discuss the computed SSM by adopting the AG89 mixture. An inspection of Table 3 reveals that the depletion efficiency of the various isotopes ranges from 9.7 to 10.7. Considering different isotopes of the same element (e.g. ^{12}C and ^{13}C or ^{20}Ne and ^{22}Ne) we see that the higher the atomic weight, the greater the depletion efficiency (see Fig. 4). A simple argument may explain this feature. Heavy nuclei, at the inner border of the solar convective envelope, move downward against the buoyancy, which is proportional to their weight A, and are decelerated by the scattering with the surrounding charge particles, which depends on the atomic number Z (we assume full ionization). Thus, the diffusion efficiency is expected to roughly scale as A/Z. Such an argument also explains why heavier isotopes of the same element are more efficiently depleted than the lighter ones. Note that the minimum depletion occurs around ^{40}Ca (see Fig. 4). Indeed, stable nuclei with $A > 40$ are progressively more neutronized, so that the ratio A/Z becomes systematically larger.

From the data reported in Table 4, we obtain ratios of the initial to present-day relative abundances very close to 1, the average value being $P = 1.003 \pm 0.004$. The corresponding average value of R is 1.552 ± 0.002 [7], in excellent agreement with its experimental determination, namely $R = 1.556 \pm 0.008$ (Palme & Jones 2004). As expected, a few exceptions are represented by elements having unstable isotopes with a half life comparable to the age of the Sun, namely: ^{40}K, ^{87}Rb, ^{138}La, ^{147}Sm, ^{176}Lu, ^{187}Re, ^{190}Pt, ^{232}Th, ^{235}U, ^{238}U [8].

Similar conclusions can be derived for the other SSMs. In particular, the average isotopic diffusion efficiency is 9.98, 10.09, 10.18, 10.91 for AG89, GN93, GS98 and Lo03, respectively, with a rather small dispersion ($\sim\pm0.8$). The differences of the average diffusion efficiency between various SSMs can be explained observing that such a quantity depends on R_{CE}^2. Indeed, the larger R_{CE}, the larger the spherical surface from which heavy elements within the convective envelope are diffused downward.

If the effects of partial ionization on microscopic diffusion and radiative acceleration were simultaneously taken into account, a slightly larger depletion efficiency of metal would be obtained. According to Turcotte et al. (1998), the increase of the depletion efficiency is less than 10% (see their Fig. 14). Since both these processes depend on the degree of ionization that is different from one nucleus to another, the scatter of the depletions is expected to increase. On the basis of the calculations of Turcotte and co-workers, the average values of P and R should

[7] The "errors" on P and R represent the maximum semi dispersion.

[8] Such elements have been excluded from the quoted average of P and R.

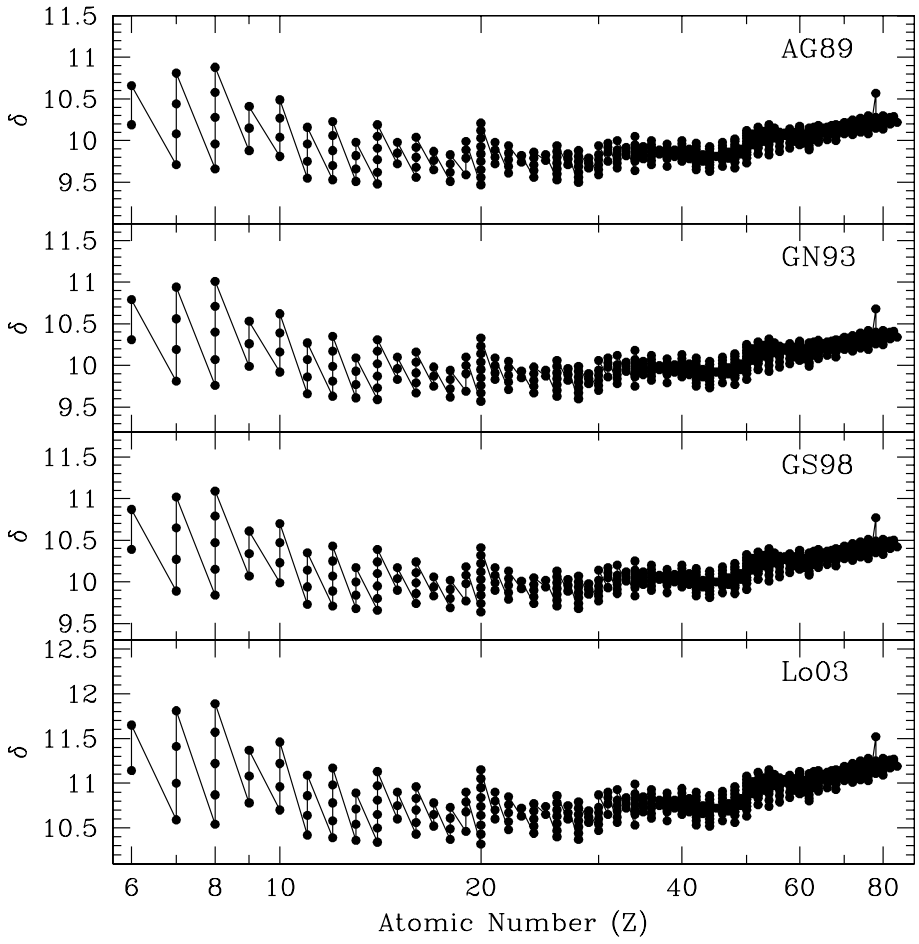

Fig. 4. Depletion efficiency $\delta = 100 \cdot (1 - X_\odot/X_{\rm in})$ as a function of the atomic number Z for all the isotopes with $Z \geq 6$. Each panel refers to a different abundance compilation, as labeled (see text). We omit the value corresponding to β-unstable isotopes, except that of the ^{190}Pt ($Z = 78$).

remain almost unaffected, while the dispersions should become about 50% larger, but within the experimental error bars.

4.2. Light isotopes ($3 < Z < 6$)

All the computed SSMs predict a stronger surface depletion for light elements than heavy ones. In particular, the ratios n(light el)/n(Si) is not conserved. For beryllium and boron, such an occurrence can be explained given that the most abundant isotopes, ^{9}Be and ^{11}B, have large A/Z values. The initial to final abundance ratio is consistent with the corresponding meteoritic to spectroscopic abundance ratio.

On the other hand, the evolution of solar lithium is one of the most debated problems in stellar modeling. During the past 4.5 Gyr, both ^{6}Li and ^{7}Li have suffered p-captures at the base of the convective external layer. Hence, not only microscopic diffusion, but also nuclear burning contributed to the modification of the photospheric lithium abundance. The major depletion takes place during the pre-Main Sequence, when, leaving the Hayashy track, the solar model develops a convective envelope, whose inner border progressively recedes in mass (see Fig. 3). The temperature at this border remains almost constant ($T_{\rm CE} \sim 3.8 \times 10^6$ K), for about 10^7 yr, so that the Li consumption is rather efficient during this phase. When the mass of the convective envelope is reduced to $\delta M_{\rm CE} \sim 0.4\ M_\odot$, $T_{\rm CE}$ starts to decrease. Then, when the solar age is about 2×10^7 yr and $\delta M_{\rm CE} \sim 0.2\ M_\odot$, the temperature becomes too low and the burning of lithium ceases. During the following Main Sequence evolution, the temperature at the base of the convective envelope always remains too low (in the four SSMs), so that the nuclear burning is inefficient (at least for ^{7}Li, the most abundant isotope). Hence, for ages greater than 10^8 yr, microscopic diffusion coupled to the convective mixing is the dominant physical process for lithium depletion. As a result, ^{6}Li is almost completely destroyed, while the present-day ^{7}Li is 3 to 5 times less than the initial one (see Fig. 5). This theoretical result implies a photospheric value of ε(Li) between 2.86 (AG89) and 3.05 (Lo03), to be compared with the corresponding spectroscopic determination, namely 1.1 ± 0.1 (Carlsson et al. 1994).

This large discrepancy represents the longstanding "solar lithium problem", for which no satisfactory explanation has been found up to now. Among the many attempts, it has been suggested that a turbulent mixing is active at the inner border of the solar convective envelope. Such a process should be driven by the expected discontinuity in the internal-rotational-velocity profile of the Sun. Indeed, according to the observation of solar surface oscillations and the relative analysis of the normal modes, it has been derived that a latitudinal-differential rotation takes place in the convective envelope, while a rigid-body rotation is active in the deep radiative interior (Goode et al. 1991). Then, there exists a thin layer, the so-called *tachocline*, located just below the convective envelope, where the external-latitudinal-differential rotation smoothly matches the internal-uniform rotation. In this case, the resulting mixing depends only on macroscopic properties of the star, as the local gradient of angular velocity, so that it equally affects all the chemical species. The effect of this mixing on SSM has been studied by Richard et al. (1996) and Brun et al. (1999 – hereafter BTZ99). In these works microscopic diffusion as well as rotational-induced mixing in the radiative zones are described by means of a diffusion

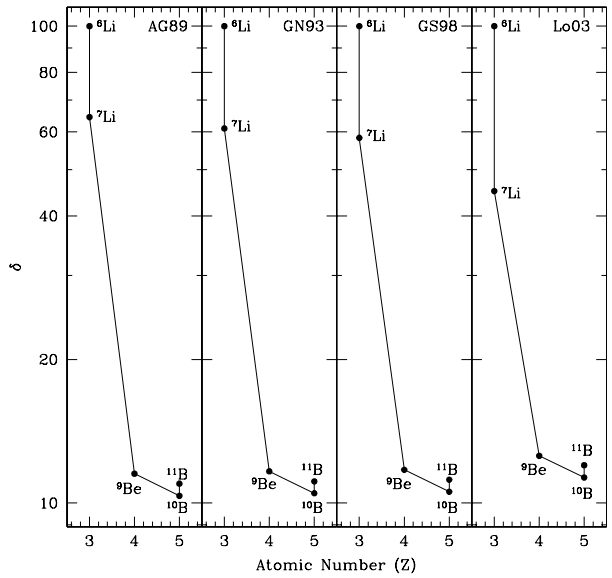

Fig. 5. The same as in Fig. 4, but for light elements ($3 \leq Z \leq 5$).

equation. In particular in BTZ99 the diffusion coefficients related to tachocline mixing are computed according to the prescription of Spiegel & Zahn (1992). The exact value of the tachocline-diffusion coefficient depends on the solar angular velocity at the base of the convective envelope, the solar differential rotation rate, the extension of the tachocline and the horizontal diffusivity.

Following the prescription of BTZ99 we have computed an additional SSM (GN93-R), accounting for mixing in the tachocline. The diffusion coefficients related to such a mixing have been calculated with Eqs. (14) and (15) of BTZ99. The evolution of the tachocline thickness has been considered by assuming that the angular velocity at the base of the convective envelope evolves according to the Skumanich law (Skumanich 1972) and introducing the dependence of the differential rotational rate on the rotation velocity derived by Donahue et al. (1996). According to helioseismic measurements (Basu 1997), we adopt $h = 0.05\ R_\odot$ for the current-age tachocline thickness. As in BTZ99, we assume a Brunt-Väissälä frequency $N^2 = 25\ \mu$Hz and the angular velocity at the base of the solar photosphere $\Omega = 0.415\ \mu$Hz.

In Table 5 we list some properties of the GN93-R model. The surface isotopic abundances and the P parameters for Li, Be and B are reported. Owing to the introduction of this extra mixing, the diffusion efficiency of all the isotopes is significantly reduced (about ∼35% less). As a consequence, a lower initial Z is required in order to reproduce the present-day Z/X, thus leading to a larger R_{CE}. Moreover, the predicted photospheric abundance of helium increases. As already discussed in BTZ99, the mixing in the tachocline smears off the sharp composition gradient just below the convective envelope, so that the resulting sound-speed profile becomes closer to the one derived from GOLF+MDI data (see Fig. 6). However, in the intermediate zone ($0.3 \leq R/R_\odot \leq 0.6$) the reproduction of the experimental sound-speed is less accurate.

The evolution of the photospheric abundance of ^{7}Li in GN93 and GN93-R models are compared in Fig. 7. Note that the tachocline penetrates to a layer where the temperature is high enough to burn ^{7}Li but not to burn ^{9}Be, ^{10}B and ^{11}B. Nevertheless, the GN93-R SSM is not able to reproduce the observed lithium depletion. Indeed, although the resulting present-day photospheric abundance is substantially smaller than the one predicted by the GN93 model (ε(Li) = 1.75), it is still larger than the observed one.

A similar conclusion was found by BTZ99 (model B_t), even if they obtained a larger lithium depletion that is marginally compatible with the observed value. The lithium depletion is greatly increased when the rotational-induced mixing is included in the computation of SSMs. The exact value of the depletion efficiency depends on the adopted parameters for the mixing in the tachocline and the relevant physical inputs.

Table 5. Some relevant quantities for models computed by including (GN93-R) and not including (GN93) the rotational-induced mixing in the tachocline: the value of the radius at the base of the convective envelope (R_{CE}), the mass extension of the convective envelope (ΔM_{CE}), the temperature (T_{CE}) and density (ρ_{CE}) at the base of the convective envelope, the central value of temperature (T_c) and density (ρ_c), the value of the mixing length parameter (α), the current-age photospheric (Z/X), X, Y and Z and their initial values, the depletion efficiency of the total metallicity ($\delta(Z)$), the abundances of the light metals lithium, beryllium and boron at the solar photosphere and the corresponding value of the P parameter (see text).

	GN93	GN93-R
$R_{CE}/R_\odot$	0.71426	0.71702
$\Delta M_{CE}/M_\odot$	0.02367	0.02298
T_{CE} (in 10^6 K)	2.18691	2.16688
ρ_{CE} (in g cm^{-3})	0.18349	0.17865
T_c (in 10^6 K)	15.7065	15.6489
ρ_c (in g cm^{-3})	154.380	153.804
α	2.25772	2.21788
$(Z/X)_\odot$	0.02439	0.02439
$X_\odot$	0.73542	0.72995
$Y_\odot$	0.24664	0.25225
$Z_\odot$	0.01793	0.01780
$(Z/X)_{in}$	0.02841	0.02692
X_{in}	0.70175	0.70680
Y_{in}	0.27831	0.27418
Z_{in}	0.01994	0.01902
$\delta(Z)$	10.08	6.41
$x(^6\mathrm{Li})_\odot$	2.365e−16	3.673e−16
$x(^7\mathrm{Li})_\odot$	4.190e−09	2.865e−10
$x(^9\mathrm{Be})_\odot$	1.699e−10	1.638e−10
$x(^{10}\mathrm{B})_\odot$	8.922e−10	8.933e−10
$x(^{11}\mathrm{B})_\odot$	3.921e−09	3.741e−09
P(Li)	2.51	36.35
P(Be)	1.02	1.05
P(B)	1.01	1.04

5. The absolute composition of stars

Once the solar composition is known, we can easily derive the absolute abundances in stars by using their spectroscopic determinations. Since these measurements are usually available for few elements only, in most cases just [Fe/H], stellar modelers commonly assume that all the other elements scale as iron. This is not the case of halo stars, for which an enhancement of the α elements (O, Ne, Mg, Si, S, Ca, Ti) with respect to iron is expected. In the following we will present the procedure to be used in these two common cases.

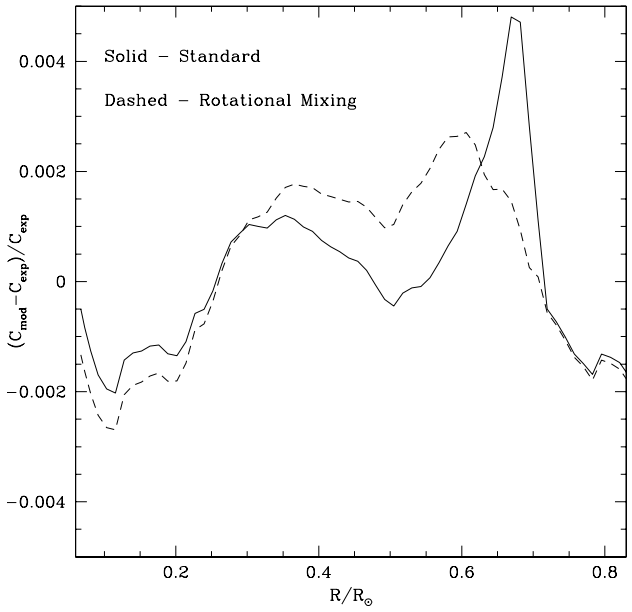

Fig. 6. Sound-speed difference between GOLF+MDI data and theoretical models including (*dashed line*) and not including (*solid line*) the rotational-induced mixing in the tachocline (see text).

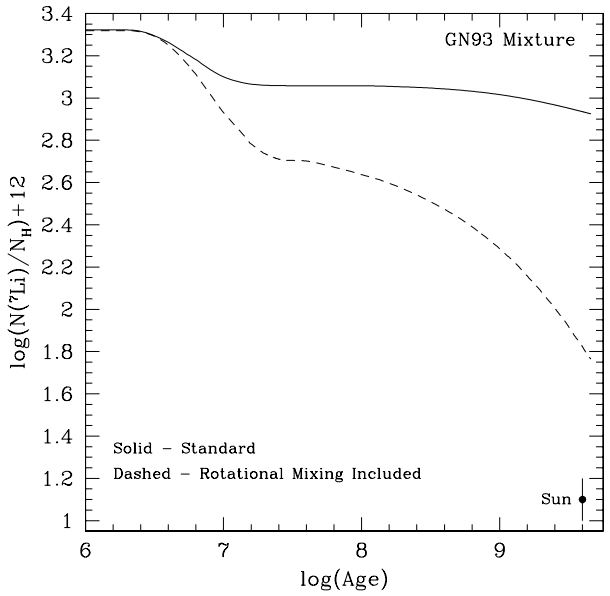

Fig. 7. Evolution of the surface lithium abundance (astronomical scale) for models with the same initial distribution of heavy elements (GN93 mixture), but computed by including (*dashed lined*) or not including (*solid line*) the rotational-induced mixing in the tachocline (see text). For comparison, the solar photospheric value is also reported.

5.1. Scaled solar compositions

If, for a given star, we know [Fe/H] and if its composition is scaled-solar, we have:

$$\left(\frac{x_j}{x_{\rm Fe}}\right)_* = \left(\frac{x_j}{x_{\rm Fe}}\right)_\odot \tag{11}$$

where the subscript $*$ refers to the star. By summing over the index j, it follows

$$\left(\frac{Z}{x_{\rm Fe}}\right)_* = \left(\frac{Z}{x_{\rm Fe}}\right)_\odot \tag{12}$$

Table 6. Values of a and b parameters in Eq. (17).

Mixture	a	b
AG89	0.70057	0.29943
GN93	0.68910	0.31090
GS98	0.68728	0.31272
Lo03	0.66946	0.33054

being, by definition:

$$\left[\frac{\rm Fe}{\rm H}\right] = \log\left(\frac{x_{\rm Fe}}{x_{\rm H}}\right)_* - \log\left(\frac{x_{\rm Fe}}{x_{\rm H}}\right)_\odot , \tag{13}$$

by combining Eqs. (12) and (13), we find:

$$\left[\frac{\rm Fe}{\rm H}\right] = \log\left(\frac{Z}{x_{\rm H}}\right)_* - \log\left(\frac{Z}{x_{\rm H}}\right)_\odot . \tag{14}$$

The last formula can be inverted to obtain the value of Z_* corresponding to the measured [Fe/H]:

$$Z_* = 10^{\rm [Fe/H]} X_* \left(\frac{Z}{X}\right)_\odot \tag{15}$$

if, in addition to [Fe/H], X_* is known, or:

$$Z_* = \frac{10^{\rm [Fe/H]}\left(\frac{Z}{X}\right)_\odot (1-Y_*)}{1+10^{\rm [Fe/H]}\left(\frac{Z}{X}\right)_\odot} \tag{16}$$

if Y_* is known[9]. Thus, the mass fraction of any element can be calculated by means of Eq. (10).

Note that both the total metallicity (Z) and the element mass fractions (x_j) depend on $(Z/X)_\odot$. For example, if a star has [Fe/H] $= -1$, its metallicity would be $Z = 2.02 \times 10^{-3}$ or $Z = 1.34 \times 10^{-3}$, depending on what solar composition is adopted, AG89 or Lo03[10], respectively.

5.2. α-enhanced compositions

The distribution of heavy elements in halo stars may differ from a scaled solar composition. The most important difference regards the enhancement, with respect to iron, of the α-elements. According to Salaris et al. (1993), when the overabundance is similar for all the α-elements, the total metallicity becomes:

$$Z_* = Z_0(a \cdot f_\alpha + b) \tag{17}$$

where Z_0 is the metallicity calculated as in the case of a scaled solar composition (from Eqs. (15) or (16)), $f_\alpha = 10^{[\alpha/{\rm Fe}]}$, $a = \sum_k (x_k/Z)_\odot$ (k = O, Ne, Mg, Si, S, Ca, Ti) and $b = 1 - a$. In Table 6 we report the coefficients a and b for the four different abundance compilations.

Also in this case, the metallicity of a given star depends on the adopted solar composition. The variation of Z is mainly due to the variation of $(Z/X)_\odot$, while the changes of a and b have negligible consequences. This occurrence has many implications for the current interpretation of the observational data. As an example, Fig. 8 shows the evolutionary tracks for $M = 0.8\ M_\odot$, [Fe/H] $= -1.4$, [α/Fe] $= 0.3$ and $Y = 0.245$, as obtained by assuming different solar compositions. Note that, although the total metallicity changes by a factor of 1.5, the effective temperature of the Main Sequence and of the RGB are only marginally

[9] Here $X = x_{\rm H}$ and $Y = x_{\rm He}$.
[10] In both cases we have used $Y = 0.245$.

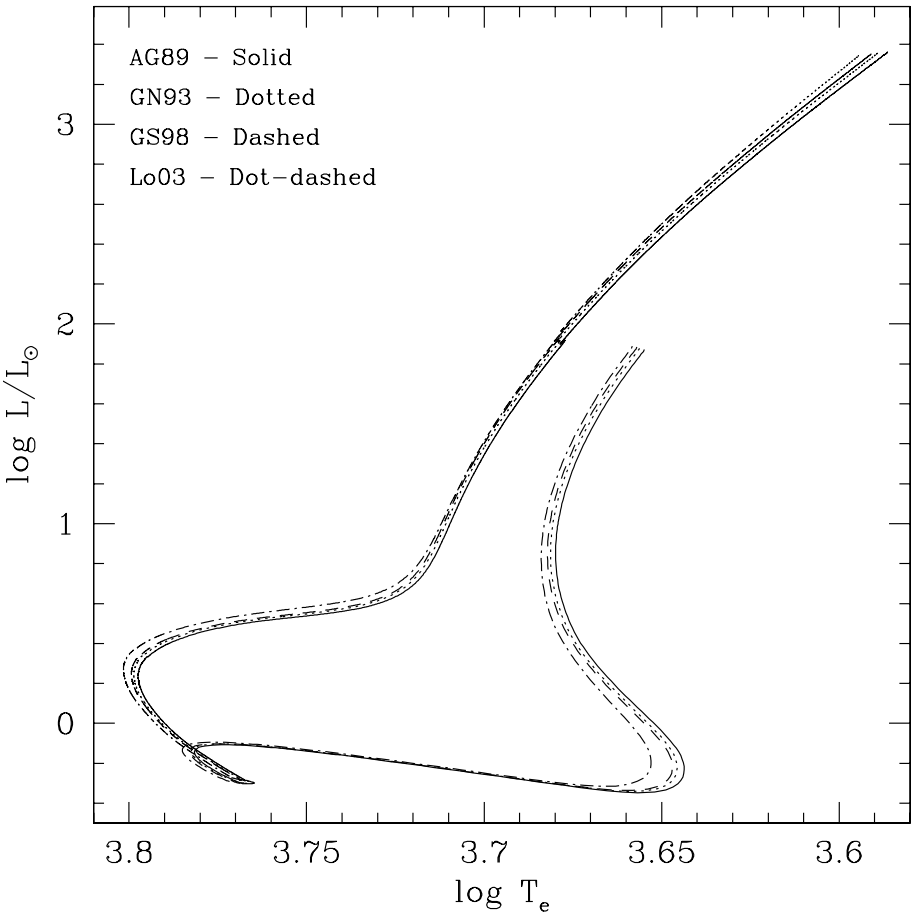

Fig. 8. HR diagram for models with $M = 0.8\ M_\odot$, $\left[\frac{\mathrm{Fe}}{\mathrm{H}}\right] = -1.4$ and $\left[\frac{\alpha}{\mathrm{Fe}}\right] = 0.3$. For each adopted distribution of heavy elements the values of α and $(Z/X)_\odot$ have been taken according to corresponding SSM (see text).

affected. In this case, the variation of Z is counterbalanced by the corresponding variation of the mixing length parameter. On the other hand, the luminosity of the Turn Off and that of the Subgiant Branch are sensitive to the variation of Z only. When this effect is transported onto the isochrones, it affects the evaluation of the ages of Globular Clusters. By means of an age-metallicity relation (see Imbriani et al. 2004 for an updated version), we find that the ages obtained with AG89 are ∼700 Myr smaller than those obtained with Lo03.

6. Summary and final remarks

In this paper we have discussed the procedure to derive the absolute abundances of the solar photosphere, of the early solar system (4.57 Gyr ago) and, in general, of stars, starting from the available data of relative elemental abundances. First, we checked the validity of the fundamental assumption made to derive a complete set of element abundances starting from different incomplete data sets, as obtained from different solar system components. It is: the evolution of the Sun has occurred preserving the relative abundances of metals. We find that, although the absolute photospheric abundances of heavy elements decrease with time mainly due to microscopic diffusion, their relative ratios remain almost unaltered. A few exceptions concern lithium and elements having long-lived radioactive isotopes. However, these elements represent a very small fraction of the total metallicity, so that we can safely conclude that a unique value of the R parameter can be used to combine photosphere and meteorite data sets (see Eq. (3)). The value estimated by means of our SSMs is in very good agreement with the one obtained by comparing spectroscopic and meteoritic measurements of a selected sample of refractory elements. The inclusion of radiative acceleration and a detailed evaluation of the partial ionization in the computation of the diffusion coefficients are not expected to modify the general conclusions of the present work, even if a more precise derivation of the absolute solar composition requires a proper treatment of these phenomena.

The absolute abundances of the solar photosphere and those of the early solar system were obtained. In particular, the computed photospheric abundances can be used to evaluate the total metallicity and the absolute composition of stars for which the [Fe/H] and [α/Fe] have been measured.

Note that the procedure described in Sect. 5 allows the determination of the current age photospheric values of the total metallicity and of the heavy element absolute abundances of stars. These quantities should not be confused with those of the material from which the star formed. The latter can be evaluated only with additional assumptions about the modification of the photospheric chemical pattern, which differs from star to star, depending on the evolutionary status, the mass and the chemical composition.

Different compilations of solar abundances imply a different Z – [Fe/H] relation for stars having scaled solar composition. When, as usual, the input composition of a (scaled-solar) stellar model is compiled starting from the measured [Fe/H], it depends on $(Z/X)_\odot$. Thus, the choice of a different solar abundance compilation leads to different Z, even if the solar iron is not changed. Such an effect is particularly severe when passing from the classical AG89 compilation to the more recent Lo03.

Recently Drake & Testa (2005) have suggested that the solar abundance of neon should be increased. Such a conclusion is based on the evidence that nearby solar-like stars have an

almost constant Ne/O ratio about 2.7 times larger than the solar value, as determined from spectra of solar wind and solar corona (see also Cunha et al. 2006). However, on the basis of the analysis of solar active region spectra, Schmeltz et al. (2005) argued that such a "enhanced-neon hypothesis" is not appliable to the Sun. If the photospheric solar neon abundance is increased according to Drake & Testa, the corresponding $(Z/X)_\odot$ should increase to 0.02016. By using this "Ne-enhanced" mixture in the computation of SSM, we obtain $Y_{\rm in} = 0.27963$, $Z_{\rm in} = 0.01653$, $Y_\odot = 0.2477$, $Z_\odot = 0.01487$ and $R_{\rm CE} = 0.7238\,R_\odot$. While we were working on the original manuscript, Antia & Basu (2006) presented an independent determination of the solar photospheric metallicity. By using the dimensionless gradient of the sound-speed, as derived by the inversion of solar oscillation frequencies, they obtain $Z_\odot = 0.0172 \pm 0.0002$, which is consistent with the theoretical value obtained by adopting the GS98 distribution of heavy elements. Unfortunately, the adopted method is only sensitive to the total value of metallicity and it is largely independent of the relative elemental abundances, so that we cannot draw a definitive conclusion concerning the distribution of individual elements. On the basis of our models we can only confirm that SSMs computed by adopting the "old" compilation of heavy elements abundances (from AG89 to GS98) better reproduce the physical properties of the current Sun as obtained by the helioseismic measurements.

Acknowledgements. Special thanks to R. Gallino for the many enlightening discussions. We also thank the anonymous referee whose suggestions allowed us to greatly improve the paper. This work has been supported by the PRIN MIUR 2004 "Nucleosynthesis in low mass stars".

References

Alexander, D. R., & Ferguson, J. W. 1994, ApJ, 437, 879
Allende Prieto, C., Lambert, D. L., & Asplund, M. 2001, ApJ, 556, L63
Allende Prieto, C., Lambert, D. L., & Asplund, M. 2002, ApJ, 573, L137
Anders, E., & Grevesse, N. 1989, Geochim. Cosmochim. Acta, 53, 197
Angulo, C., Arnould, M., Rayet, M., et al. 1999, Nucl. Phys. A, 656, 3
Antia, H. M., & Basu, S. 2006, ApJ, 644, 1292
Asplund, M. 2000, A&A, 359, 755
Asplund, M., Nordlund, A., Trampedach, R., & Stein, R. F. 2000, A&A, 359, 743
Asplund, M., Grevesse, N., Sauval, A. J., Allende Prieto, C., & Kiselman, D. 2004, A&A, 417, 751
Bahcall, J. N., Basu, S., & Pinsonneault, M. 1998, Phys. Lett. B, 433, 128
Bahcall, J. N., Serenelli, A. M., & Pinsonneault, M. 2004, ApJ, 614, 464
Bahcall, J. N., Basu, S., Pinsonneault, M., & Serenelli, A. M. 2005, ApJ, 618, 1049
Basu, S. 1997, MNRAS, 288, 572
Basu, S., & Antia, H. M. 1997, MNRAS, 287, 189
Basu, S., & Antia, H. M. 2004, ApJ, 606, L85
Bono, G., Caputo, F., Cassisi, S., Castellani, V., & Marconi, M. 1997, ApJ, 479, 279
Bono, G., Caputo, F., Cassisi, S., Marconi, M., Piersanti, L., & Tornambé, A. 2000, ApJ, 543, 955
Brun, A. S., Turck-Chièze, S., & Zahn, J. P. 1999, ApJ, 535, 1032
Cameron, A. G. W. 1973, Space Sci. Rev., 15, 121
Cameron, A. G. W. 1982, in Essays in Nuclear Astrophysics, ed. C. A. Barnes, D. D. Clayton, & D. N. Schramm (Cambridge Univ. Press), 23
Carlsson, M., Rutten, R. J., Brules, J. H. M. J., & Shchukina, N. G. 1994, A&A, 288, 860
Casella, C., Costantini, H., Lemut, A., et al. 2002, Nucl. Phys. A, 706, 203
Caughlan, G. R., & Fowler, W. A. 1988, Atom. Data Nucl. Data Tables, 40, 283
Charbonnel, C., Däppen, W., Schaerer, D., et al. 1999, A&AS, 135, 405
Chieffi, A., Limongi, M., & Straniero, O. 1998, ApJ, 502, 737
Clarke, F. W. 1889, Bull. Phil. Soc. Washington, 11, 131
Coc, A., Porquet, M. G., & Nowacki, F. 2000, Phys. Rev. C, 61, 015801
Cox, J. P., & Giuli, R. T. 1968, in Principles of Stellar Evolution, Vol. 1 (New York: Gordon & Breach), 281
Cunha, K., Hubeny, I., & Lanz, T. 2006 [arXiv:astro-ph/0606738]
D'Antona, F., & Mazzitelli, I. 1984, A&A, 138, 431
Dewitt, H. E., Graboske, H. C., & Cooper, M. S. 1973, ApJ, 181, 439
Dominguez, I., Chieffi, A., Limongi, M., & Straniero, O. 1999, ApJ, 524, 226
Donahue, R. A., Saar, S. H., & Baliunas, S. L. 1996, ApJ, 466, 384
Drake, J. J., & Testa, P. 2005, Nature, 436, 525
Esteban, C., & Peimbert, M. 1995, Rev. Mex. Astron. Astrofis. SC, 3, 133
Girardi, L., & Bertelli, G. 1998, MNRAS, 300, 533
Goode, P. R., Dziembowski, W. A., Korzennik, S. G., & Rhodes, E. J. Jr. 1991, ApJ, 367, 649
Graboske, H. C., Dewitt, H. E., Grossman, A. S., & Cooper, M. S. 1973, ApJ, 181, 457
Grevesse, N. 1984, Phys. Scr., 8, 49
Grevesse, N., & Noels, A. 1993, in Origin and evolution of the elements, ed. N. Prantzos, E. Vangioni-Flam, & M. Cassé (Cambridge University Press), 15
Grevesse, N., & Sauval, A. J. 1998, Space Sci. Rev., 85, 161
Iglesias, C. A., & Rogers, F. J. 1996, ApJ, 464, 943
Imbriani, G., Costantini, H., Formicola, A., et al. 2004, A&A, 420, 625
Imbriani, G., Costantini, H., Formicola, A., et al. 2005, EPJA, 25, 455
Itoh, N., Totsuji, H., & Ichimaru, S. 1977, ApJ, 218, 477
Itoh, N., Totsuji, H., Ichimaru, S., & Dewitt, H. E. 1979, ApJ, 234, 1079
Kim, Y. C., Demarque, P., Yi, S. K., & Alexander, D. R. 2002, ApJS, 143, 499
Kosovichev, A. G., Schou, J., Scherrer, P. H., et al. 1997, Sol. Phys., 170, 43
Lazrek, M., Baudin, F., Bertello, L., et al. 1997, Sol. Phys., 175, 227
Lodders, K. 2003, ApJ, 591, 1220
Maeder, A., & Meynet, G. 2001, A&A, 373, 555
Mihalas, D., Hummer, D. G., Mihalas, B. W., & Daeppen, W. 1990, ApJ, 350, 300
Oda, T., Hino, M., Muto, K., Takahara, M., & Sato, K. 1994, Atom. Data Nucl. Data Tables, 56, 231
Palme, H., & Beer, H. 1993, in Landolt Börnstein Group VI, Astronomy and Astrophysics, Vol. 2A, ed. H. H. Voigt (Berlin: Springer), 196
Palme, H., & Jones, A. 2004, in Meteorites, Comets and Planets, Treatise on Geochemistry, Vol. 1, ed. A. M. Davis (Amsterdam: Elsevier), 4
Pietrinferni, A., Cassisi, S., Salaris, M., & Castelli, F. 2004, ApJ, 612, 168
Pinsonneault, M. H., Kawaler, S. D., Sofia, S., & Demarque, P. 1989, ApJ, 338, 424
Pols, O. R., Schroder, K. P., Hurley, J. R., Tout, C. A., & Eggleton, P. P. 1998, MNRAS, 298, 525
Prada Moroni, P. G., & Straniero, O. 2002, ApJ, 581, 585
Richard, O., Vauclair, S., Charbonnel, C., & Dziembowski, W. A. 1996, A&A, 312, 1000
Rogers, F. J., & Iglesias, C. A. 1992, ApJS, 79, 507
Rogers, F. J., Swenson, F. J., & Iglesias, C. A. 1996, ApJ, 456, 902
Salaris, M., Chieffi, A., & Straniero, O. 1993, ApJ, 414, 580
Salaris, M., degl'Innocenti, S., & Weiss, A. 1997, ApJ, 479, 665
Schmelz, J. T., Nasraoui, K., Roames, J. K., Lippner, L. A., & Garst, J. W. 2005, ApJ, 634, L197
Skumanich, A. 1972, ApJ, 171, 565
Spergel, D. N., Verde, L., Peiris, H. V., et al. 2003, ApJS, 148, 175
Spiegel, E. A., & Zahn, J. P. 1992, A&A, 265, 106
Straniero, O. 1988, A&AS, 76, 157
Straniero, O., Chieffi, A., & Limongi, M. 1997, ApJ, 490, 425
Suess, H. E., & Urey, H. C. 1956, Rev. Mod. Phys., 28, 53
Thoul, A. A., Bahcall, J. N., & Loeb, A. 1994, ApJ, 421, 828
Turcotte, S., Richer, J., Michaud, G., Iglesias, C. A., & Rogers, F. J. 1998, ApJ, 504, 539

Online Material

Table 3. From left to right, mass fraction abundances for all the considered isotopes of the proto-solar nebula (x_{in}) and at the solar photosphere ($x_\odot$). The depletion efficiency δ is also reported. The initial and final values of the metallicity and the corresponding depletion efficiency are reported in the last row (see text).

			AG89			GN93			GS98			Lo03		
El	Z	A	x_{in}	$x_\odot$	δ	x_{in}	$x_\odot$	δ	x_{in}	$x_\odot$	δ	x_{in}	$x_\odot$	δ
H	1	1.007825	0.6973	0.7310	–4.84	0.7017	0.7354	–4.80	0.7038	0.7376	–4.80	0.7127	0.7479	–4.95
		2.014102	2.3709E-05	2.0297E-17	100.00	2.3860E-05	2.0738E-17	100.00	2.3930E-05	2.1005E-17	100.00	1.3826E-05	2.3034E-17	100.00
He	2	3.016029	3.9904E-05	6.9378E-05	–73.86	3.9520E-05	6.9141E-05	–74.95	3.9385E-05	6.9056E-05	–75.34	4.5235E-05	6.0081E-05	–32.82
		4.002603	0.2810	0.2494	11.24	0.2783	0.2466	11.39	0.2773	0.2455	11.49	0.2725	0.2388	12.36
Li	3	6.015123	7.4216E-10	2.4842E-16	100.00	7.4719E-10	2.3647E-16	100.00	7.5013E-10	2.4387E-16	100.00	7.2349E-10	1.1082E-13	99.98
		7.016005	1.0676E-08	3.7929E-09	64.47	1.0749E-08	4.1896E-09	61.02	1.0791E-08	4.4981E-09	58.32	1.0276E-08	5.6411E-09	45.10
Be	4	9.012182	1.9100E-10	1.6900E-10	11.52	1.9229E-10	1.6988E-10	11.65	1.9305E-10	1.7038E-10	11.74	1.9268E-10	1.6847E-10	12.56
B	5	10.012937	1.2179E-09	1.0918E-09	10.35	9.9665E-10	8.9224E-10	10.48	1.0006E-09	8.9492E-10	10.56	9.9465E-10	8.8207E-10	11.32
		11.009305	5.3900E-09	4.7986E-09	10.97	4.4108E-09	3.9211E-09	11.10	4.4282E-09	3.9326E-09	11.19	4.4242E-09	3.8932E-09	12.00
C	6	12.000000	3.4719E-03	3.1180E-03	10.19	3.4159E-03	3.0637E-03	10.31	3.2004E-03	2.8679E-03	10.39	2.4230E-03	2.1531E-03	11.14
		13.003355	4.1845E-05	3.7384E-05	10.66	4.1169E-05	3.6729E-05	10.79	3.8573E-05	3.4379E-05	10.87	2.9412E-05	2.5985E-05	11.65
N	7	14.003074	1.2613E-03	1.1342E-03	10.08	1.0562E-03	9.4863E-04	10.19	9.4507E-04	8.4802E-04	10.27	7.8457E-04	6.9828E-04	11.00
		15.000109	4.9633E-06	4.4449E-06	10.44	4.1563E-06	3.7172E-06	10.56	3.7188E-06	3.3229E-06	10.65	3.0898E-06	2.7373E-06	11.41
O	8	15.994915	1.0943E-02	9.8529E-03	9.96	9.5956E-03	8.6290E-03	10.07	8.7857E-03	7.8939E-03	10.15	6.5006E-03	5.7937E-03	10.87
		16.999132	4.4300E-06	3.9748E-06	10.28	3.8845E-06	3.4807E-06	10.40	3.5567E-06	3.1841E-06	10.47	2.5762E-06	2.2870E-06	11.22
		17.999161	2.4687E-05	2.2075E-05	10.58	2.1648E-05	1.9329E-05	10.71	1.9820E-05	1.7682E-05	10.79	1.4665E-05	1.2969E-05	11.57
F	9	18.998403	4.6229E-07	4.1538E-07	10.15	5.5956E-07	5.0213E-07	10.26	4.6725E-07	4.1893E-07	10.34	4.5574E-07	4.0525E-07	11.08
Ne	10	19.992440	1.8429E-03	1.6621E-03	9.81	1.8131E-03	1.6333E-03	9.92	1.8203E-03	1.6383E-03	9.99	1.1457E-03	1.0231E-03	10.70
		20.993847	4.7032E-06	4.2309E-06	10.04	4.6273E-06	4.1573E-06	10.16	4.6455E-06	4.1701E-06	10.23	2.8841E-06	2.5680E-06	10.96
		21.991385	1.4802E-04	1.3282E-04	10.27	1.4563E-04	1.3050E-04	10.39	1.4620E-04	1.3090E-04	10.47	9.2670E-05	8.2276E-05	11.22
Na	11	22.989769	3.7821E-05	3.4056E-05	9.96	3.9871E-05	3.5857E-05	10.07	3.9117E-05	3.5149E-05	10.14	3.8154E-05	3.4008E-05	10.86
Mg	12	23.985042	5.8037E-04	5.2406E-04	9.70	5.8431E-04	5.2698E-04	9.81	5.8660E-04	5.2862E-04	9.89	5.7217E-04	5.1161E-04	10.58
		24.985837	7.6540E-05	6.8976E-05	9.88	7.7059E-05	6.9359E-05	9.99	7.7362E-05	6.9572E-05	10.07	7.5479E-05	6.7340E-05	10.78
		25.982593	8.7632E-05	7.8817E-05	10.06	8.8226E-05	7.9251E-05	10.17	8.8573E-05	7.9494E-05	10.25	8.6353E-05	7.6871E-05	10.98
Al	13	26.981539	6.5654E-05	5.9207E-05	9.82	6.4594E-05	5.8181E-05	9.93	6.7904E-05	6.1111E-05	10.00	6.4725E-05	5.7790E-05	10.71
Si	14	27.976927	7.3768E-04	6.6669E-04	9.62	7.4268E-04	6.7043E-04	9.73	7.6296E-04	6.8817E-04	9.80	7.4417E-04	6.6607E-04	10.50
		28.976495	3.8686E-05	3.4908E-05	9.77	3.8948E-05	3.5103E-05	9.87	4.0012E-05	3.6031E-05	9.95	3.9137E-05	3.4967E-05	10.65
		29.973770	2.6564E-05	2.3932E-05	9.91	2.6744E-05	2.4064E-05	10.02	2.7475E-05	2.4701E-05	10.10	2.6687E-05	2.3801E-05	10.81
P	15	30.973762	9.2723E-06	8.3710E-06	9.72	7.0814E-06	6.3854E-06	9.83	9.1585E-06	8.2515E-06	9.90	6.9342E-06	6.1989E-06	10.60
S	16	31.972071	4.5581E-04	4.1223E-04	9.56	3.9968E-04	3.6105E-04	9.67	3.9212E-04	3.5393E-04	9.74	3.9136E-04	3.5055E-04	10.43
		32.971459	3.7102E-06	3.3510E-06	9.68	3.2533E-06	2.9349E-06	9.79	3.1918E-06	2.8769E-06	9.86	3.1857E-06	2.8492E-06	10.56
		33.967867	2.1456E-05	1.9353E-05	9.80	1.8814E-05	1.6949E-05	9.91	1.8458E-05	1.6614E-05	9.99	1.8445E-05	1.6472E-05	10.70
		35.967081	1.0793E-07	9.7086E-08	10.04	9.4637E-08	8.5024E-08	10.16	9.2847E-08	8.3342E-08	10.24	7.8770E-08	7.0133E-08	10.96
Cl	17	34.968853	3.9753E-06	3.5918E-06	9.65	6.7968E-06	6.1338E-06	9.75	4.1116E-06	3.7075E-06	9.83	4.0104E-06	3.5884E-06	10.52
		36.965903	1.3438E-06	1.2112E-06	9.87	2.2976E-06	2.0682E-06	9.98	1.3899E-06	1.2501E-06	10.06	1.3556E-06	1.2096E-06	10.78
Ar	18	35.967545	8.8597E-05	8.0170E-05	9.51	8.1349E-05	7.3525E-05	9.62	6.1952E-05	5.5950E-05	9.69	8.9796E-05	8.0480E-05	10.37
		37.962732	1.7547E-05	1.5841E-05	9.72	1.6112E-05	1.4528E-05	9.83	1.2270E-05	1.1055E-05	9.91	1.7232E-05	1.5404E-05	10.61
	18	39.962383	0.0000E+00	3.9045E-10		0.0000E+00	3.8336E-10		0.0000E+00	3.9327E-10		2.9013E-08	2.6228E-08	10.84
K	19	38.963707	3.9495E-06	3.5709E-06	9.59	3.8857E-06	3.5090E-06	9.69	3.9919E-06	3.6020E-06	9.77	3.7184E-06	3.3295E-06	10.46
		39.963998	5.0691E-10	2.4288E-11	95.21	4.9873E-10	2.3694E-11	95.25	5.1236E-10	2.4200E-11	95.28	4.7733E-10	2.1314E-11	95.53
		40.961826	2.9964E-07	2.7031E-07	9.79	2.9480E-07	2.6562E-07	9.90	3.0286E-07	2.7265E-07	9.98	2.8211E-07	2.5197E-07	10.68
Ca	20	39.962591	6.8290E-05	6.1826E-05	9.47	7.1993E-05	6.5102E-05	9.57	7.0631E-05	6.3821E-05	9.64	6.7323E-05	6.0372E-05	10.32
		41.958618	4.7854E-07	4.3235E-07	9.65	5.0449E-07	4.5525E-07	9.76	4.9495E-07	4.4626E-07	9.84	4.7177E-07	4.2208E-07	10.53
		42.958767	1.0223E-07	9.2267E-08	9.75	1.0777E-07	9.7153E-08	9.85	1.0573E-07	9.5234E-08	9.93	1.0078E-07	9.0063E-08	10.64
		43.955482	1.6163E-06	1.4573E-06	9.84	1.7039E-06	1.5344E-06	9.95	1.6717E-06	1.5041E-06	10.03	1.5934E-06	1.4223E-06	10.74

Table 3. continued.

			AG89			GN93			GS98			Lo03		
El	Z	A	x_{in}	$x_{\odot}$	δ	x_{in}	$x_{\odot}$	δ	x_{in}	$x_{\odot}$	δ	x_{in}	$x_{\odot}$	δ
		45.953693	3.2402E-09	2.9153E-09	10.03	3.4159E-09	3.0696E-09	10.14	3.3513E-09	3.0088E-09	10.22	3.1944E-09	2.8446E-09	10.95
		47.952534	1.5807E-07	1.4193E-07	10.21	1.6664E-07	1.4943E-07	10.33	1.6349E-07	1.4647E-07	10.41	1.5583E-07	1.3845E-07	11.15
Sc	21	44.955912	4.4564E-08	4.0234E-08	9.72	5.3940E-08	4.8641E-08	9.83	4.6091E-08	4.1528E-08	9.90	4.3933E-08	3.9274E-08	10.60
Ti	22	45.952632	2.5211E-07	2.2790E-07	9.61	3.1227E-07	2.8194E-07	9.71	2.6075E-07	2.3523E-07	9.79	2.6225E-07	2.3476E-07	10.48
		46.951763	2.3505E-07	2.1228E-07	9.69	2.9114E-07	2.6262E-07	9.80	2.4311E-07	2.1911E-07	9.87	2.4158E-07	2.1603E-07	10.57
		47.947946	2.4267E-06	2.1896E-06	9.77	3.0058E-06	2.7088E-06	9.88	2.5099E-06	2.2600E-06	9.96	2.4455E-06	2.1846E-06	10.67
		48.947870	1.8462E-07	1.6643E-07	9.85	2.2868E-07	2.0589E-07	9.97	1.9095E-07	1.7178E-07	10.04	1.8317E-07	1.6346E-07	10.76
		49.944791	1.8496E-07	1.6658E-07	9.94	2.2909E-07	2.0607E-07	10.05	1.9130E-07	1.7193E-07	10.13	1.7916E-07	1.5972E-07	10.85
V	23	49.947158	1.0535E-09	9.5091E-10	9.74	1.0129E-09	9.1315E-10	9.85	1.0648E-09	9.5915E-10	9.92	1.0374E-09	9.2707E-10	10.63
		50.943960	4.2875E-07	3.8665E-07	9.82	4.1222E-07	3.7128E-07	9.93	4.3335E-07	3.8999E-07	10.01	4.2268E-07	3.7737E-07	10.72
Cr	24	49.946044	8.3692E-07	7.5689E-07	9.56	8.2341E-07	7.4378E-07	9.67	8.6561E-07	7.8127E-07	9.74	8.2512E-07	7.3900E-07	10.44
		51.940507	1.6784E-05	1.5154E-05	9.71	1.6513E-05	1.4891E-05	9.82	1.7359E-05	1.5641E-05	9.90	1.6546E-05	1.4792E-05	10.60
		52.940649	1.9398E-06	1.7499E-06	9.79	1.9085E-06	1.7195E-06	9.90	2.0063E-06	1.8062E-06	9.97	1.9122E-06	1.7079E-06	10.69
		53.938880	4.9196E-07	4.4343E-07	9.86	4.8402E-07	4.3573E-07	9.98	5.0882E-07	4.5768E-07	10.05	4.8493E-07	4.3271E-07	10.77
Mn	25	54.938045	1.4999E-05	1.3535E-05	9.76	1.0940E-05	9.8598E-06	9.87	1.5160E-05	1.3653E-05	9.94	1.4450E-05	1.2911E-05	10.65
Fe	26	53.939611	8.1570E-05	7.3798E-05	9.53	8.0253E-05	7.2522E-05	9.63	8.0569E-05	7.2748E-05	9.71	7.9195E-05	7.0960E-05	10.40
		55.934937	1.3376E-03	1.2084E-03	9.66	1.3161E-03	1.1874E-03	9.77	1.3212E-03	1.1911E-03	9.85	1.2892E-03	1.1532E-03	10.55
		56.935394	3.2659E-05	2.9480E-05	9.73	3.2132E-05	2.8969E-05	9.84	3.2258E-05	2.9059E-05	9.92	3.0305E-05	2.7085E-05	10.63
		57.933276	4.2294E-06	3.8149E-06	9.80	4.1611E-06	3.7486E-06	9.91	4.1775E-06	3.7602E-06	9.99	4.1038E-06	3.6645E-06	10.70
Co	27	58.933195	3.8597E-06	3.4850E-06	9.71	3.9764E-06	3.5859E-06	9.82	3.9011E-06	3.5152E-06	9.89	3.8051E-06	3.4017E-06	10.60
Ni	28	57.935343	5.6672E-05	5.1289E-05	9.50	5.7056E-05	5.1576E-05	9.60	5.7280E-05	5.1737E-05	9.68	5.4444E-05	4.8800E-05	10.37
		59.930786	2.2412E-05	2.0255E-05	9.62	2.2564E-05	2.0368E-05	9.73	2.2653E-05	2.0432E-05	9.81	2.1694E-05	1.9415E-05	10.51
		60.931056	9.8653E-07	8.9097E-07	9.69	9.9322E-07	8.9592E-07	9.80	9.9712E-07	8.9870E-07	9.87	9.5876E-07	8.5736E-07	10.58
		61.928345	3.1855E-06	2.8749E-06	9.75	3.2071E-06	2.8908E-06	9.86	3.2197E-06	2.8998E-06	9.94	3.1070E-06	2.7762E-06	10.65
		63.927966	8.3354E-07	7.5120E-07	9.88	8.3919E-07	7.5533E-07	9.99	8.4249E-07	7.5766E-07	10.07	8.1680E-07	7.2867E-07	10.79
Cu	29	62.929597	6.5308E-07	5.8995E-07	9.67	5.7266E-07	5.1668E-07	9.78	6.9120E-07	6.2311E-07	9.85	6.5887E-07	5.8933E-07	10.56
		64.927789	3.0033E-07	2.7093E-07	9.79	2.6335E-07	2.3727E-07	9.90	3.1786E-07	2.8615E-07	9.98	3.0294E-07	2.7055E-07	10.69
Zn	30	63.929142	1.1189E-06	1.0116E-06	9.59	1.0040E-06	9.0664E-07	9.70	1.1842E-06	1.0685E-06	9.77	1.1288E-06	1.0106E-06	10.47
		65.926033	6.6200E-07	5.9773E-07	9.71	5.9400E-07	5.3568E-07	9.82	7.0064E-07	6.3132E-07	9.89	6.6783E-07	5.9703E-07	10.60
		66.927127	9.8760E-08	8.9114E-08	9.77	8.8616E-08	7.9862E-08	9.88	1.0452E-07	9.4120E-08	9.95	9.9630E-08	8.9002E-08	10.67
		67.924844	4.5838E-07	4.1334E-07	9.83	4.1130E-07	3.7041E-07	9.94	4.8513E-07	4.3655E-07	10.02	4.6242E-07	4.1278E-07	10.73
		69.925319	1.5603E-08	1.4052E-08	9.94	1.4001E-08	1.2592E-08	10.06	1.6514E-08	1.4840E-08	10.14	1.5741E-08	1.4030E-08	10.87
Ga	31	68.925574	4.5030E-08	4.0642E-08	9.75	4.5336E-08	4.0867E-08	9.86	4.5514E-08	4.0993E-08	9.93	4.3383E-08	3.8764E-08	10.65
		70.924701	3.0752E-08	2.7720E-08	9.86	3.0961E-08	2.7872E-08	9.98	3.1082E-08	2.7958E-08	10.05	2.9627E-08	2.6435E-08	10.77
Ge	32	69.924247	4.9269E-08	4.4504E-08	9.67	4.9603E-08	4.4751E-08	9.78	4.9798E-08	4.4890E-08	9.86	5.1483E-08	4.6045E-08	10.56
		71.922076	6.7734E-08	6.1108E-08	9.78	6.8193E-08	6.1445E-08	9.89	6.8461E-08	6.1636E-08	9.97	6.8984E-08	6.1613E-08	10.69
		72.923459	1.9550E-08	1.7627E-08	9.84	1.9683E-08	1.7724E-08	9.95	1.9760E-08	1.7779E-08	10.03	1.9513E-08	1.7416E-08	10.75
		73.921178	9.2738E-08	8.3564E-08	9.89	9.3366E-08	8.4021E-08	10.01	9.3733E-08	8.4281E-08	10.08	9.2127E-08	8.2168E-08	10.81
		75.921403	2.0354E-08	1.8318E-08	10.00	2.0492E-08	1.8418E-08	10.12	2.0573E-08	1.8475E-08	10.20	1.9596E-08	1.7454E-08	10.93
As	33	74.921596	1.4151E-08	1.2762E-08	9.82	1.4247E-08	1.2833E-08	9.93	1.4303E-08	1.2872E-08	10.01	1.3020E-08	1.1624E-08	10.72
Se	34	73.922476	1.2051E-09	1.0889E-09	9.64	1.3930E-09	1.2572E-09	9.75	1.3985E-09	1.2611E-09	9.83	1.2860E-09	1.1506E-09	10.53
		75.919214	1.2487E-08	1.1271E-08	9.75	1.4435E-08	1.3012E-08	9.86	1.4491E-08	1.3052E-08	9.93	1.3728E-08	1.2266E-08	10.65
		76.919914	1.0682E-08	9.6353E-09	9.80	1.2347E-08	1.1124E-08	9.91	1.2396E-08	1.1158E-08	9.99	1.1336E-08	1.0122E-08	10.70
		77.917309	3.3596E-08	3.0287E-08	9.85	3.8835E-08	3.4965E-08	9.96	3.8987E-08	3.5074E-08	10.04	3.5748E-08	3.1901E-08	10.76
		79.916521	7.3438E-08	6.6131E-08	9.95	8.4890E-08	7.6342E-08	10.07	8.5224E-08	7.6578E-08	10.14	7.7432E-08	6.9010E-08	10.88
		81.916699	1.3097E-08	1.1780E-08	10.05	1.5139E-08	1.3598E-08	10.18	1.5198E-08	1.3641E-08	10.25	1.3129E-08	1.1686E-08	10.99
Br	35	78.918337	1.3924E-08	1.2562E-08	9.78	1.4018E-08	1.2632E-08	9.89	1.4073E-08	1.2671E-08	9.97	1.3108E-08	1.1708E-08	10.68
		80.916291	1.3884E-08	1.2512E-08	9.88	1.3978E-08	1.2581E-08	9.99	1.4033E-08	1.2620E-08	10.07	1.3072E-08	1.1661E-08	10.79

Table 3. continued.

			AG89			GN93			GS98			Lo03		
El	Z	A	x_{in}	$x_{\odot}$	δ	x_{in}	$x_{\odot}$	δ	x_{in}	$x_{\odot}$	δ	x_{in}	$x_{\odot}$	δ
Kr	36	77.920388	3.7999E-10	3.4226E-10	9.93	4.5994E-10	4.1373E-10	10.05	4.6175E-10	4.1502E-10	10.12	4.6999E-10	4.1899E-10	10.85
		79.916379	2.4276E-09	2.1918E-09	9.71	2.9384E-09	2.6498E-09	9.82	2.9500E-09	2.6580E-09	9.90	2.9512E-09	2.6380E-09	10.61
		81.913484	1.2834E-08	1.1575E-08	9.81	1.5534E-08	1.3993E-08	9.92	1.5595E-08	1.4036E-08	10.00	1.5125E-08	1.3503E-08	10.72
		82.914136	1.3013E-08	1.1730E-08	9.86	1.5751E-08	1.4180E-08	9.97	1.5813E-08	1.4224E-08	10.05	1.5178E-08	1.3543E-08	10.77
		83.911507	6.5573E-08	5.9078E-08	9.91	7.9371E-08	7.1415E-08	10.02	7.9683E-08	7.1636E-08	10.10	7.5672E-08	6.7479E-08	10.83
		85.910611	2.0478E-08	1.8430E-08	10.00	2.4787E-08	2.2278E-08	10.12	2.4884E-08	2.2347E-08	10.20	2.3430E-08	2.0868E-08	10.93
Rb	37	84.911790	1.2402E-08	1.1182E-08	9.84	1.2777E-08	1.1505E-08	9.95	1.2827E-08	1.1541E-08	10.03	1.1676E-08	1.0421E-08	10.75
		86.909181	4.8961E-09	4.1098E-09	16.06	5.0441E-09	4.2282E-09	16.18	5.0639E-09	4.2412E-09	16.25	4.6095E-09	3.8280E-09	16.95
Sr	38	83.913424	3.2227E-10	2.9105E-10	9.69	3.1706E-10	2.8601E-10	9.79	3.1831E-10	2.8689E-10	9.87	3.1492E-10	2.8160E-10	10.58
		85.909260	5.8462E-09	5.2746E-09	9.78	5.7519E-09	5.1831E-09	9.89	5.7745E-09	5.1991E-09	9.96	5.7018E-09	5.0927E-09	10.68
		86.908877	4.1340E-09	3.7279E-09	9.82	4.0672E-09	3.6631E-09	9.94	4.0832E-09	3.6744E-09	10.01	4.3346E-09	3.8694E-09	10.73
		87.905612	4.9783E-08	4.4871E-08	9.87	4.8980E-08	4.4090E-08	9.98	4.9173E-08	4.4227E-08	10.06	4.8883E-08	4.3612E-08	10.78
Y	39	88.905848	1.1888E-08	1.0723E-08	9.81	1.2248E-08	1.1033E-08	9.92	1.2296E-08	1.1067E-08	10.00	1.1720E-08	1.0464E-08	10.72
Zr	40	89.904704	1.5183E-08	1.3703E-08	9.75	1.5286E-08	1.3779E-08	9.86	1.5346E-08	1.3821E-08	9.94	1.5318E-08	1.3686E-08	10.65
		90.905646	3.3479E-09	3.0201E-09	9.79	3.3706E-09	3.0368E-09	9.90	3.3839E-09	3.0462E-09	9.98	3.3783E-09	3.0169E-09	10.70
		91.905041	5.1737E-09	4.6648E-09	9.83	5.2087E-09	4.6905E-09	9.95	5.2292E-09	4.7050E-09	10.02	5.2180E-09	4.6572E-09	10.75
		93.906315	5.3572E-09	4.8258E-09	9.92	5.3935E-09	4.8521E-09	10.04	5.4147E-09	4.8671E-09	10.11	5.4044E-09	4.8184E-09	10.84
		95.908273	8.8147E-10	7.9329E-10	10.00	8.8744E-10	7.9757E-10	10.13	8.9093E-10	8.0005E-10	10.20	8.8892E-10	7.9168E-10	10.94
Nb	41	92.906378	1.8804E-09	1.6965E-09	9.78	1.8931E-09	1.7059E-09	9.89	1.9005E-09	1.7111E-09	9.97	2.0326E-09	1.8154E-09	10.68
Mo	42	91.906811	1.0022E-09	9.0558E-10	9.65	1.0325E-09	9.3189E-10	9.75	1.0366E-09	9.3473E-10	9.83	1.1083E-09	9.9160E-10	10.53
		93.905088	6.3830E-10	5.7622E-10	9.73	6.5759E-10	5.9293E-10	9.83	6.6018E-10	5.9475E-10	9.91	7.0579E-10	6.3080E-10	10.62
		94.905842	1.1103E-09	1.0018E-09	9.77	1.1438E-09	1.0309E-09	9.88	1.1483E-09	1.0340E-09	9.95	1.2281E-09	1.0971E-09	10.67
		95.904679	1.1755E-09	1.0602E-09	9.81	1.2111E-09	1.0909E-09	9.92	1.2158E-09	1.0943E-09	9.99	1.2999E-09	1.1606E-09	10.72
		96.906021	6.8006E-10	6.1310E-10	9.85	7.0062E-10	6.3083E-10	9.96	7.0337E-10	6.3278E-10	10.04	7.5264E-10	6.7165E-10	10.76
		97.905408	1.7360E-09	1.5644E-09	9.89	1.7885E-09	1.6096E-09	10.00	1.7955E-09	1.6146E-09	10.08	1.9205E-09	1.7130E-09	10.81
		99.907477	7.0700E-10	6.3653E-10	9.97	7.2837E-10	6.5489E-10	10.09	7.3123E-10	6.5692E-10	10.16	7.8232E-10	6.9706E-10	10.90
Ru	44	95.907598	2.8183E-10	2.5469E-10	9.63	2.9035E-10	2.6210E-10	9.73	2.9149E-10	2.6289E-10	9.81	2.7895E-10	2.4962E-10	10.52
		97.905287	9.7985E-11	8.8475E-11	9.71	1.0095E-10	9.1043E-11	9.81	1.0134E-10	9.1321E-11	9.89	9.6022E-11	8.5843E-11	10.60
		98.905939	6.6868E-10	6.0353E-10	9.74	6.8890E-10	6.2103E-10	9.85	6.9160E-10	6.2293E-10	9.93	6.6223E-10	5.9173E-10	10.64
		99.904219	6.7011E-10	6.0456E-10	9.78	6.9037E-10	6.2208E-10	9.89	6.9308E-10	6.2399E-10	9.97	6.6055E-10	5.8995E-10	10.69
		100.905582	9.1318E-10	8.2351E-10	9.82	9.4079E-10	8.4735E-10	9.93	9.4449E-10	8.4995E-10	10.01	9.0344E-10	8.0648E-10	10.73
		101.904349	1.7142E-09	1.5453E-09	9.86	1.7661E-09	1.5899E-09	9.97	1.7730E-09	1.5948E-09	10.05	1.6874E-09	1.5056E-09	10.78
		103.905433	1.0344E-09	9.3161E-10	9.93	1.0656E-09	9.5850E-10	10.05	1.0698E-09	9.6146E-10	10.13	1.0154E-09	9.0512E-10	10.86
Rh	45	102.905504	1.0201E-09	9.2002E-10	9.81	1.0509E-09	9.4667E-10	9.92	1.0550E-09	9.4957E-10	10.00	1.0776E-09	9.6207E-10	10.72
Pd	46	101.905607	4.2798E-11	3.8652E-11	9.69	4.3088E-11	3.8869E-11	9.79	4.3258E-11	3.8988E-11	9.87	4.4181E-11	3.9506E-11	10.58
		103.904036	4.7193E-10	4.2586E-10	9.76	4.7513E-10	4.2824E-10	9.87	4.7699E-10	4.2955E-10	9.95	4.8718E-10	4.3522E-10	10.66
		104.905085	9.5498E-10	8.6141E-10	9.80	9.6145E-10	8.6620E-10	9.91	9.6523E-10	8.6885E-10	9.99	9.8583E-10	8.8029E-10	10.71
		105.903486	1.1799E-09	1.0638E-09	9.83	1.1879E-09	1.0697E-09	9.95	1.1925E-09	1.0730E-09	10.02	1.2180E-09	1.0871E-09	10.75
		107.903892	1.1637E-09	1.0484E-09	9.91	1.1716E-09	1.0541E-09	10.02	1.1762E-09	1.0574E-09	10.10	1.2013E-09	1.0712E-09	10.83
		109.905153	5.0596E-10	4.5548E-10	9.98	5.0939E-10	4.5795E-10	10.10	5.1140E-10	4.5936E-10	10.18	5.2231E-10	4.6532E-10	10.91
Ag	47	106.905097	7.7598E-10	7.0003E-10	9.79	7.8124E-10	7.0393E-10	9.90	7.8431E-10	7.0608E-10	9.97	7.8282E-10	6.9910E-10	10.69
		108.904752	7.3441E-10	6.6201E-10	9.86	7.3938E-10	6.6566E-10	9.97	7.4229E-10	6.6770E-10	10.05	7.4087E-10	6.6105E-10	10.77
Cd	48	105.906458	6.1380E-11	5.5442E-11	9.67	6.1796E-11	5.5756E-11	9.77	6.2039E-11	5.5924E-11	9.86	6.0511E-11	5.4118E-11	10.56
		107.904184	4.4527E-11	4.0189E-11	9.74	4.4829E-11	4.0414E-11	9.85	4.5005E-11	4.0537E-11	9.93	4.3897E-11	3.9225E-11	10.64
		109.903002	6.3645E-10	5.7400E-10	9.81	6.4077E-10	5.7719E-10	9.92	6.4329E-10	5.7895E-10	10.00	6.2745E-10	5.6017E-10	10.72
		110.904178	6.5819E-10	5.9338E-10	9.85	6.6265E-10	5.9666E-10	9.96	6.6526E-10	5.9848E-10	10.04	6.4888E-10	5.7904E-10	10.76
		111.902758	1.2520E-09	1.1282E-09	9.88	1.2604E-09	1.1345E-09	10.00	1.2654E-09	1.1379E-09	10.07	1.2342E-09	1.1009E-09	10.80
		112.904402	6.3970E-10	5.7626E-10	9.92	6.4403E-10	5.7942E-10	10.03	6.4657E-10	5.8120E-10	10.11	6.3065E-10	5.6228E-10	10.84
		113.903359	1.5173E-09	1.3663E-09	9.95	1.5276E-09	1.3738E-09	10.07	1.5336E-09	1.3780E-09	10.15	1.4958E-09	1.3331E-09	10.88

Table 3. continued.

			AG89			GN93			GS98			Lo03		
El	Z	A	x_{in}	$x_{\odot}$	δ	x_{in}	$x_{\odot}$	δ	x_{in}	$x_{\odot}$	δ	x_{in}	$x_{\odot}$	δ
		115.904756	4.0251E-10	3.6218E-10	10.02	4.0524E-10	3.6414E-10	10.14	4.0683E-10	3.6526E-10	10.22	3.9681E-10	3.5333E-10	10.96
In	49	112.904058	2.5845E-11	2.3302E-11	9.84	2.6020E-11	2.3432E-11	9.95	2.6122E-11	2.3503E-11	10.03	2.5408E-11	2.2676E-11	10.75
		114.903878	5.8538E-10	5.2740E-10	9.90	5.8935E-10	5.3030E-10	10.02	5.9167E-10	5.3193E-10	10.10	5.7717E-10	5.1468E-10	10.83
Sn	50	111.904820	1.2110E-10	1.0932E-10	9.73	1.2192E-10	1.0994E-10	9.83	1.2240E-10	1.1027E-10	9.91	1.1643E-10	1.0406E-10	10.63
		113.902779	8.3486E-11	7.5309E-11	9.79	8.4052E-11	7.5730E-11	9.90	8.4382E-11	7.5960E-11	9.98	8.0431E-11	7.1824E-11	10.70
		114.903342	4.3324E-11	3.9066E-11	9.83	4.3617E-11	3.9284E-11	9.94	4.3789E-11	3.9403E-11	10.02	4.1738E-11	3.7256E-11	10.74
		115.901741	1.8741E-09	1.6893E-09	9.86	1.8868E-09	1.6986E-09	9.97	1.8942E-09	1.7038E-09	10.05	1.8053E-09	1.6107E-09	10.78
		116.902952	9.9753E-10	8.9884E-10	9.89	1.0043E-09	9.0380E-10	10.01	1.0082E-09	9.0656E-10	10.09	9.6153E-10	8.5754E-10	10.82
		117.901603	3.1757E-09	2.8604E-09	9.93	3.1972E-09	2.8761E-09	10.04	3.2098E-09	2.8849E-09	10.12	3.0602E-09	2.7281E-09	10.85
		118.903308	1.1356E-09	1.0225E-09	9.96	1.1433E-09	1.0281E-09	10.08	1.1478E-09	1.0312E-09	10.16	1.0938E-09	9.7468E-10	10.89
		119.902195	4.3470E-09	3.9126E-09	9.99	4.3764E-09	3.9339E-09	10.11	4.3936E-09	3.9459E-09	10.19	4.1875E-09	3.7299E-09	10.93
		121.903439	6.2803E-10	5.6486E-10	10.06	6.3228E-10	5.6791E-10	10.18	6.3477E-10	5.6965E-10	10.26	6.0465E-10	5.3812E-10	11.00
		123.905274	7.9751E-10	7.1678E-10	10.12	8.0292E-10	7.2061E-10	10.25	8.0607E-10	7.2283E-10	10.33	7.6859E-10	6.8345E-10	11.08
Sb	51	120.903816	6.1271E-10	5.5176E-10	9.95	6.0283E-10	5.4216E-10	10.06	6.0520E-10	5.4381E-10	10.14	6.6060E-10	5.8874E-10	10.88
		122.904214	4.6297E-10	4.1662E-10	10.01	4.5550E-10	4.0935E-10	10.13	4.5729E-10	4.1060E-10	10.21	5.0221E-10	4.4721E-10	10.95
Te	52	119.904019	1.5110E-11	1.3623E-11	9.84	1.5213E-11	1.3699E-11	9.95	1.5272E-11	1.3740E-11	10.03	1.5889E-11	1.4180E-11	10.76
		121.903044	4.3867E-10	3.9522E-10	9.91	4.4165E-10	3.9740E-10	10.02	4.4338E-10	3.9861E-10	10.10	4.3802E-10	3.9059E-10	10.83
		122.904270	1.5316E-10	1.3794E-10	9.94	1.5420E-10	1.3870E-10	10.05	1.5481E-10	1.3912E-10	10.13	1.5405E-10	1.3731E-10	10.86
		123.902818	8.2581E-10	7.4349E-10	9.97	8.3141E-10	7.4756E-10	10.09	8.3468E-10	7.4984E-10	10.16	8.2370E-10	7.3391E-10	10.90
		124.904431	1.2417E-09	1.1176E-09	10.00	1.2502E-09	1.1237E-09	10.12	1.2551E-09	1.1271E-09	10.20	1.2309E-09	1.0963E-09	10.94
		125.903312	3.3301E-09	2.9961E-09	10.03	3.3527E-09	3.0123E-09	10.15	3.3659E-09	3.0215E-09	10.23	3.2938E-09	2.9324E-09	10.97
		127.904463	5.6826E-09	5.1090E-09	10.09	5.7211E-09	5.1365E-09	10.22	5.7436E-09	5.1522E-09	10.30	5.5946E-09	4.9767E-09	11.04
		129.906224	6.1790E-09	5.5515E-09	10.16	6.2209E-09	5.5811E-09	10.28	6.2454E-09	5.5982E-09	10.36	6.0609E-09	5.3872E-09	11.12
I	53	126.904473	3.3088E-09	2.9783E-09	9.99	3.3312E-09	2.9946E-09	10.11	3.3443E-09	3.0037E-09	10.19	3.6600E-09	3.2602E-09	10.92
Xe	54	123.905895	2.0515E-11	1.8499E-11	9.83	1.7989E-11	1.6202E-11	9.93	1.8060E-11	1.6251E-11	10.01	2.4756E-11	2.2098E-11	10.74
		125.904268	1.8606E-11	1.6767E-11	9.89	1.6315E-11	1.4684E-11	10.00	1.6379E-11	1.4729E-11	10.08	2.1840E-11	1.9480E-11	10.81
		127.903531	3.8328E-10	3.4516E-10	9.95	3.3609E-10	3.0227E-10	10.06	3.3741E-10	3.0319E-10	10.14	4.4177E-10	3.9371E-10	10.88
		128.904779	4.8224E-09	4.3412E-09	9.98	4.2286E-09	3.8018E-09	10.09	4.2452E-09	3.8133E-09	10.17	5.4824E-09	4.8842E-09	10.91
		129.903508	7.7322E-10	6.9583E-10	10.01	6.7801E-10	6.0936E-10	10.13	6.8068E-10	6.1120E-10	10.21	8.8125E-10	7.8478E-10	10.95
		130.905082	3.8852E-09	3.4951E-09	10.04	3.4068E-09	3.0607E-09	10.16	3.4202E-09	3.0700E-09	10.24	4.4199E-09	3.9346E-09	10.98
		131.904153	4.7830E-09	4.3014E-09	10.07	4.1940E-09	3.7667E-09	10.19	4.2105E-09	3.7781E-09	10.27	5.3853E-09	4.7921E-09	11.02
		133.905394	1.7883E-09	1.6072E-09	10.13	1.5681E-09	1.4073E-09	10.25	1.5743E-09	1.4116E-09	10.33	2.0035E-09	1.7814E-09	11.08
		135.907219	1.4766E-09	1.3261E-09	10.19	1.2948E-09	1.1612E-09	10.32	1.2999E-09	1.1647E-09	10.40	1.6564E-09	1.4717E-09	11.15
Cs	55	132.905452	1.4117E-09	1.2701E-09	10.03	1.4544E-09	1.3068E-09	10.15	1.4601E-09	1.3108E-09	10.23	1.3917E-09	1.2391E-09	10.97
Ba	56	129.906310	1.7994E-11	1.6218E-11	9.87	1.8538E-11	1.6688E-11	9.98	1.8611E-11	1.6739E-11	10.06	1.7706E-11	1.5796E-11	10.79
		131.905056	1.7409E-11	1.5680E-11	9.93	1.7935E-11	1.6135E-11	10.04	1.8006E-11	1.6183E-11	10.12	1.7197E-11	1.5330E-11	10.86
		133.904508	4.2293E-10	3.8069E-10	9.99	4.3571E-10	3.9170E-10	10.10	4.3742E-10	3.9288E-10	10.18	4.1694E-10	3.7140E-10	10.92
		134.905689	1.1621E-09	1.0457E-09	10.02	1.1972E-09	1.0759E-09	10.13	1.2019E-09	1.0791E-09	10.22	1.1456E-09	1.0201E-09	10.96
		135.904576	1.3948E-09	1.2547E-09	10.05	1.4370E-09	1.2909E-09	10.16	1.4426E-09	1.2948E-09	10.25	1.3749E-09	1.2238E-09	10.99
		136.905827	2.0091E-09	1.8067E-09	10.08	2.0698E-09	1.8588E-09	10.19	2.0779E-09	1.8644E-09	10.28	1.9810E-09	1.7626E-09	11.02
		137.905247	1.2921E-08	1.1615E-08	10.10	1.3312E-08	1.1950E-08	10.23	1.3364E-08	1.1986E-08	10.31	1.2738E-08	1.1330E-08	11.06
La	57	137.907112	1.5674E-12	1.3658E-12	12.86	1.6524E-12	1.4380E-12	12.97	1.6589E-12	1.4423E-12	13.05	1.5655E-12	1.3497E-12	13.79
		138.906353	1.7723E-09	1.5939E-09	10.06	1.8684E-09	1.6781E-09	10.18	1.8757E-09	1.6832E-09	10.27	1.7472E-09	1.5548E-09	11.01
Ce	58	135.907143	8.4760E-12	7.6357E-12	9.91	8.9356E-12	8.0402E-12	10.02	8.9707E-12	8.0642E-12	10.11	8.5656E-12	7.6374E-12	10.84
		137.905985	1.1317E-11	1.0188E-11	9.97	1.1930E-11	1.0728E-11	10.08	1.1977E-11	1.0760E-11	10.16	1.1729E-11	1.0450E-11	10.90
		139.905439	4.0632E-09	3.6559E-09	10.03	4.2836E-09	3.8492E-09	10.14	4.3004E-09	3.8607E-09	10.22	4.1931E-09	3.7333E-09	10.97
		141.909244	5.1611E-10	4.6408E-10	10.08	5.4410E-10	4.8860E-10	10.20	5.4624E-10	4.9006E-10	10.28	5.3442E-10	4.7547E-10	11.03
Pr	59	140.907653	6.8411E-10	6.1578E-10	9.99	7.2121E-10	6.4836E-10	10.10	7.2405E-10	6.5030E-10	10.19	7.0622E-10	6.2907E-10	10.92

Table 3. continued.

			AG89			GN93			GS98			Lo03		
El	Z	A	x_{in}	$x_{\odot}$	δ	x_{in}	$x_{\odot}$	δ	x_{in}	$x_{\odot}$	δ	x_{in}	$x_{\odot}$	δ
Nd	60	141.907723	9.1548E-10	8.2436E-10	9.95	9.6512E-10	8.6802E-10	10.06	9.6892E-10	8.7060E-10	10.15	9.2457E-10	8.2396E-10	10.88
		142.909814	4.1391E-10	3.7260E-10	9.98	4.3635E-10	3.9232E-10	10.09	4.3807E-10	3.9349E-10	10.18	4.1790E-10	3.7229E-10	10.91
		143.910087	8.1445E-10	7.3294E-10	10.01	8.5861E-10	7.7172E-10	10.12	8.6199E-10	7.7402E-10	10.21	8.2266E-10	7.3262E-10	10.95
		144.912574	2.8601E-10	2.5731E-10	10.04	3.0152E-10	2.7092E-10	10.15	3.0270E-10	2.7172E-10	10.23	2.8853E-10	2.5686E-10	10.98
		145.913117	5.9644E-10	5.3642E-10	10.06	6.2878E-10	5.6478E-10	10.18	6.3125E-10	5.6647E-10	10.26	6.0099E-10	5.3484E-10	11.01
		147.916893	2.0260E-10	1.8210E-10	10.12	2.1358E-10	1.9172E-10	10.24	2.1442E-10	1.9229E-10	10.32	2.0367E-10	1.8113E-10	11.07
		149.920891	2.0106E-10	1.8062E-10	10.17	2.1197E-10	1.9015E-10	10.29	2.1280E-10	1.9072E-10	10.38	2.0176E-10	1.7930E-10	11.13
Sm	62	143.911999	3.3547E-11	3.0231E-11	9.89	3.4561E-11	3.1109E-11	9.99	3.4697E-11	3.1201E-11	10.08	3.2788E-11	2.9246E-11	10.80
		146.914898	1.6571E-10	1.4456E-10	12.76	1.7072E-10	1.4875E-10	12.87	1.7139E-10	1.4919E-10	12.95	1.6329E-10	1.4096E-10	13.68
		147.914823	1.2569E-10	1.1313E-10	9.99	1.2948E-10	1.1641E-10	10.10	1.2999E-10	1.1675E-10	10.19	1.2326E-10	1.0979E-10	10.93
		148.917185	1.5453E-10	1.3905E-10	10.02	1.5920E-10	1.4308E-10	10.13	1.5983E-10	1.4350E-10	10.22	1.5255E-10	1.3584E-10	10.96
		149.917276	8.3421E-11	7.5042E-11	10.04	8.5943E-11	7.7214E-11	10.16	8.6281E-11	7.7443E-11	10.24	8.2014E-11	7.3003E-11	10.99
		151.919732	3.0501E-10	2.7422E-10	10.10	3.1423E-10	2.8214E-10	10.21	3.1547E-10	2.8298E-10	10.30	3.0117E-10	2.6790E-10	11.05
		153.922209	2.6274E-10	2.3607E-10	10.15	2.7068E-10	2.4289E-10	10.27	2.7174E-10	2.4361E-10	10.35	2.5961E-10	2.3078E-10	11.11
Eu	63	150.919850	2.0154E-10	1.8137E-10	10.01	2.0764E-10	1.8662E-10	10.12	2.0845E-10	1.8718E-10	10.21	1.9873E-10	1.7698E-10	10.95
		152.921230	2.2301E-10	2.0057E-10	10.06	2.2976E-10	2.0638E-10	10.17	2.3066E-10	2.0699E-10	10.26	2.1982E-10	1.9562E-10	11.01
Gd	64	151.919791	2.8763E-12	2.5894E-12	9.98	3.0323E-12	2.7265E-12	10.08	3.0442E-12	2.7346E-12	10.17	2.9437E-12	2.6226E-12	10.91
		153.920866	3.1765E-11	2.8579E-11	10.03	3.3487E-11	3.0092E-11	10.14	3.3619E-11	3.0181E-11	10.23	3.2058E-11	2.8542E-11	10.97
		154.922622	2.1706E-10	1.9523E-10	10.05	2.2883E-10	2.0557E-10	10.16	2.2973E-10	2.0617E-10	10.25	2.1897E-10	1.9489E-10	11.00
		155.922123	3.0215E-10	2.7169E-10	10.08	3.1853E-10	2.8607E-10	10.19	3.1978E-10	2.8691E-10	10.28	3.0476E-10	2.7115E-10	11.03
		156.923960	2.3249E-10	2.0899E-10	10.10	2.4509E-10	2.2005E-10	10.22	2.4606E-10	2.2070E-10	10.31	2.3456E-10	2.0863E-10	11.06
		157.924104	3.7136E-10	3.3374E-10	10.13	3.9150E-10	3.5138E-10	10.25	3.9304E-10	3.5242E-10	10.33	3.7455E-10	3.3303E-10	11.08
		159.927054	3.3095E-10	2.9726E-10	10.18	3.4890E-10	3.1296E-10	10.30	3.5027E-10	3.1389E-10	10.39	3.3392E-10	2.9671E-10	11.14
Tb	65	158.925347	2.7377E-10	2.4613E-10	10.10	2.8862E-10	2.5915E-10	10.21	2.8975E-10	2.5991E-10	10.30	2.6990E-10	2.4009E-10	11.05
Dy	66	155.924270	1.0257E-12	9.2162E-13	10.15	1.0813E-12	9.7034E-13	10.26	1.0856E-12	9.7319E-13	10.35	1.0112E-12	8.9890E-13	11.10
		157.924409	1.7255E-12	1.5527E-12	10.01	1.8191E-12	1.6350E-12	10.12	1.8262E-12	1.6398E-12	10.21	1.7011E-12	1.5148E-12	10.95
		159.925198	4.2592E-11	3.8306E-11	10.06	4.4901E-11	4.0334E-11	10.17	4.5078E-11	4.0452E-11	10.26	4.1989E-11	3.7367E-11	11.01
		160.926933	3.4635E-10	3.1141E-10	10.09	3.6513E-10	3.2789E-10	10.20	3.6657E-10	3.2885E-10	10.29	3.4145E-10	3.0377E-10	11.04
		161.926798	4.7014E-10	4.2259E-10	10.11	4.9563E-10	4.4495E-10	10.23	4.9758E-10	4.4625E-10	10.31	4.6348E-10	4.1220E-10	11.06
		162.928731	4.6173E-10	4.1493E-10	10.14	4.8677E-10	4.3687E-10	10.25	4.8868E-10	4.3815E-10	10.34	4.5520E-10	4.0471E-10	11.09
		163.929175	5.2595E-10	4.7251E-10	10.16	5.5447E-10	4.9748E-10	10.28	5.5665E-10	4.9894E-10	10.37	5.1847E-10	4.6081E-10	11.12
Ho	67	164.930322	4.2024E-10	3.7768E-10	10.13	4.3294E-10	3.8860E-10	10.24	4.3464E-10	3.8974E-10	10.33	4.2394E-10	3.7696E-10	11.08
Er	68	161.928774	1.6280E-12	1.4652E-12	10.00	1.7162E-12	1.5428E-12	10.10	1.7230E-12	1.5473E-12	10.19	1.6446E-12	1.4647E-12	10.93
		163.929200	1.8953E-11	1.7049E-11	10.05	1.9981E-11	1.7951E-11	10.16	2.0059E-11	1.8004E-11	10.25	1.9553E-11	1.7404E-11	10.99
		165.930293	4.0037E-10	3.5995E-10	10.10	4.2208E-10	3.7900E-10	10.21	4.2374E-10	3.8011E-10	10.30	4.1343E-10	3.6776E-10	11.04
		166.932048	2.7512E-10	2.4728E-10	10.12	2.9003E-10	2.6036E-10	10.23	2.9118E-10	2.6112E-10	10.32	2.8376E-10	2.5234E-10	11.07
		167.932370	3.2319E-10	2.9041E-10	10.14	3.4072E-10	3.0577E-10	10.26	3.4206E-10	3.0666E-10	10.35	3.3351E-10	2.9649E-10	11.10
		169.935464	1.8183E-10	1.6330E-10	10.19	1.9169E-10	1.7193E-10	10.31	1.9244E-10	1.7243E-10	10.40	1.8801E-10	1.6703E-10	11.15
Tm	69	168.934213	1.8362E-10	1.6505E-10	10.11	1.9357E-10	1.7378E-10	10.22	1.9433E-10	1.7429E-10	10.31	1.8102E-10	1.6099E-10	11.06
Yb	70	167.933890	1.6051E-12	1.4417E-12	10.18	1.6536E-12	1.4834E-12	10.30	1.6602E-12	1.4877E-12	10.39	1.6193E-12	1.4388E-12	11.14
		169.934762	3.7220E-11	3.3468E-11	10.08	3.8345E-11	3.4438E-11	10.19	3.8496E-11	3.4539E-11	10.28	3.7425E-11	3.3298E-11	11.03
		170.936326	1.7554E-10	1.5780E-10	10.10	1.8084E-10	1.6237E-10	10.21	1.8155E-10	1.6284E-10	10.30	1.7683E-10	1.5729E-10	11.05
		171.936381	2.7040E-10	2.4302E-10	10.13	2.7857E-10	2.5005E-10	10.24	2.7967E-10	2.5078E-10	10.33	2.7191E-10	2.4178E-10	11.08
		172.938211	2.0019E-10	1.7987E-10	10.15	2.0624E-10	1.8508E-10	10.26	2.0706E-10	1.8562E-10	10.35	2.0208E-10	1.7964E-10	11.11
		173.938862	3.9721E-10	3.5680E-10	10.17	4.0921E-10	3.6711E-10	10.29	4.1082E-10	3.6819E-10	10.38	4.0109E-10	3.5643E-10	11.13
		175.942572	1.6046E-10	1.4406E-10	10.22	1.6531E-10	1.4822E-10	10.34	1.6596E-10	1.4865E-10	10.43	1.6264E-10	1.4444E-10	11.19
Lu	71	174.940772	1.8100E-10	1.6265E-10	10.14	1.8648E-10	1.6735E-10	10.25	1.8721E-10	1.6784E-10	10.34	1.7439E-10	1.5504E-10	11.10
		175.942686	4.8402E-12	3.9792E-12	17.79	4.9865E-12	4.0940E-12	17.90	5.0061E-12	4.1058E-12	17.99	4.6523E-12	3.7819E-12	18.71
Hf	72	173.940040	1.2193E-12	1.0966E-12	10.07	1.2854E-12	1.1546E-12	10.17	1.2905E-12	1.1580E-12	10.26	1.3801E-12	1.2282E-12	11.01

Table 3. continued.

			AG89			GN93			GS98			Lo03		
El	Z	A	x_{in}	$x_{\odot}$	δ	x_{in}	$x_{\odot}$	δ	x_{in}	$x_{\odot}$	δ	x_{in}	$x_{\odot}$	δ
		175.941409	3.9634E-11	3.5626E-11	10.11	4.1783E-11	3.7512E-11	10.22	4.1947E-11	3.7622E-11	10.31	4.5243E-11	4.0238E-11	11.06
		176.943221	1.4246E-10	1.2802E-10	10.13	1.5018E-10	1.3479E-10	10.25	1.5077E-10	1.3519E-10	10.34	1.6117E-10	1.4330E-10	11.09
		177.943699	2.1018E-10	1.8883E-10	10.16	2.2158E-10	1.9882E-10	10.27	2.2245E-10	1.9940E-10	10.36	2.3779E-10	2.1136E-10	11.11
		178.945816	1.0553E-10	9.4788E-11	10.18	1.1125E-10	9.9801E-11	10.29	1.1169E-10	1.0009E-10	10.38	1.1939E-10	1.0609E-10	11.14
		179.946550	2.7330E-10	2.4542E-10	10.20	2.8812E-10	2.5840E-10	10.32	2.8926E-10	2.5915E-10	10.41	3.0921E-10	2.7468E-10	11.17
Ta	73	179.947465	2.3470E-14	2.1088E-14	10.15	1.2985E-14	1.1653E-14	10.26	1.3036E-14	1.1687E-14	10.35	1.3337E-14	1.1856E-14	11.11
		180.947996	1.9665E-10	1.7665E-10	10.17	1.0880E-10	9.7611E-11	10.28	1.0923E-10	9.7895E-11	10.38	1.0902E-10	9.6885E-11	11.13
W	74	179.946704	9.0215E-13	8.1107E-13	10.10	9.2943E-13	8.3458E-13	10.21	9.3308E-13	8.3702E-13	10.30	8.0095E-13	7.1249E-13	11.04
		181.948204	1.8454E-10	1.6583E-10	10.14	1.9012E-10	1.7063E-10	10.25	1.9087E-10	1.7113E-10	10.34	1.7913E-10	1.5926E-10	11.10
		182.950223	1.0089E-10	9.0640E-11	10.16	1.0394E-10	9.3263E-11	10.28	1.0435E-10	9.3535E-11	10.37	9.7294E-11	8.6474E-11	11.12
		183.950931	2.1758E-10	1.9542E-10	10.19	2.2415E-10	2.0107E-10	10.30	2.2503E-10	2.0165E-10	10.39	2.0942E-10	1.8608E-10	11.15
		185.954364	2.0510E-10	1.8412E-10	10.23	2.1130E-10	1.8944E-10	10.35	2.1213E-10	1.8999E-10	10.44	1.9639E-10	1.7440E-10	11.20
Re	75	184.952955	1.0378E-10	9.3244E-11	10.16	1.0692E-10	9.5943E-11	10.27	1.0734E-10	9.6224E-11	10.36	1.0469E-10	9.3059E-11	11.11
		186.955753	1.7559E-10	1.4599E-10	16.86	1.8090E-10	1.5020E-10	16.97	1.8161E-10	1.5063E-10	17.06	1.7715E-10	1.4563E-10	17.79
Os	76	183.952490	6.3999E-13	5.7546E-13	10.08	6.5933E-13	5.9215E-13	10.19	6.6193E-13	5.9389E-13	10.28	7.1019E-13	6.3187E-13	11.03
		185.953838	5.6788E-11	5.1038E-11	10.13	5.8505E-11	5.2516E-11	10.24	5.8735E-11	5.2670E-11	10.32	5.7731E-11	5.1335E-11	11.08
		186.955750	5.7817E-11	5.1950E-11	10.15	5.9564E-11	5.3454E-11	10.26	5.9799E-11	5.3611E-11	10.35	5.9930E-11	5.3276E-11	11.10
		187.955838	4.8317E-10	4.3404E-10	10.17	4.9778E-10	4.4660E-10	10.28	4.9973E-10	4.4791E-10	10.37	4.8693E-10	4.3275E-10	11.13
		188.958147	5.8801E-10	5.2809E-10	10.19	6.0579E-10	5.4337E-10	10.30	6.0817E-10	5.4495E-10	10.39	5.9685E-10	5.3028E-10	11.15
		189.958447	9.6930E-10	8.7032E-10	10.21	9.9860E-10	8.9548E-10	10.33	1.0025E-09	8.9809E-10	10.42	9.7576E-10	8.6669E-10	11.18
		191.961481	1.5212E-09	1.3652E-09	10.25	1.5672E-09	1.4047E-09	10.37	1.5734E-09	1.4088E-09	10.46	1.5314E-09	1.3595E-09	11.23
Ir	77	190.960594	1.3454E-09	1.2084E-09	10.18	1.3545E-09	1.2151E-09	10.30	1.3598E-09	1.2186E-09	10.38	1.3253E-09	1.1777E-09	11.14
		192.962926	2.2853E-09	2.0516E-09	10.22	2.3007E-09	2.0628E-09	10.34	2.3098E-09	2.0689E-09	10.43	2.2539E-09	2.0017E-09	11.19
Pt	78	189.959930	9.3038E-13	8.3202E-13	10.57	9.5850E-13	8.5612E-13	10.68	9.6227E-13	8.5864E-13	10.77	1.0076E-12	8.9153E-13	11.52
		191.961038	5.7743E-11	5.1881E-11	10.15	5.9489E-11	5.3383E-11	10.26	5.9723E-11	5.3540E-11	10.35	5.8451E-11	5.1957E-11	11.11
		193.962680	2.4610E-09	2.2101E-09	10.19	2.5354E-09	2.2740E-09	10.31	2.5453E-09	2.2807E-09	10.40	2.4877E-09	2.2102E-09	11.16
		194.964791	2.5414E-09	2.2817E-09	10.22	2.6182E-09	2.3477E-09	10.33	2.6285E-09	2.3546E-09	10.42	2.5662E-09	2.2792E-09	11.18
		195.964952	1.9045E-09	1.7095E-09	10.24	1.9620E-09	1.7589E-09	10.35	1.9697E-09	1.7641E-09	10.44	1.9244E-09	1.7088E-09	11.21
		197.967893	5.4893E-10	4.9251E-10	10.28	5.6552E-10	5.0673E-10	10.40	5.6775E-10	5.0821E-10	10.49	5.5173E-10	4.8964E-10	11.25
Au	79	196.966569	1.0730E-09	9.6345E-10	10.21	1.1311E-09	1.0144E-09	10.32	1.1356E-09	1.0174E-09	10.41	1.1076E-09	9.8389E-10	11.17
Hg	80	195.965814	2.9799E-12	2.6778E-12	10.14	3.2895E-12	2.9524E-12	10.25	3.3025E-12	2.9612E-12	10.33	3.6151E-12	3.2142E-12	11.09
		197.966769	1.9561E-10	1.7570E-10	10.18	2.1594E-10	1.9371E-10	10.29	2.1679E-10	1.9429E-10	10.38	2.3725E-10	2.1082E-10	11.14
		198.968280	3.3279E-10	2.9885E-10	10.20	3.6737E-10	3.2948E-10	10.31	3.6881E-10	3.3045E-10	10.40	4.0363E-10	3.5857E-10	11.16
		199.968326	4.5782E-10	4.1103E-10	10.22	5.0539E-10	4.5316E-10	10.33	5.0738E-10	4.5449E-10	10.42	5.5527E-10	4.9316E-10	11.19
		200.970302	2.6259E-10	2.3570E-10	10.24	2.8987E-10	2.5985E-10	10.36	2.9101E-10	2.6062E-10	10.44	3.1848E-10	2.8278E-10	11.21
		201.970643	5.9788E-10	5.3654E-10	10.26	6.6001E-10	5.9151E-10	10.38	6.6260E-10	5.9325E-10	10.47	7.2515E-10	6.4369E-10	11.23
		203.973494	1.3881E-10	1.2451E-10	10.30	1.5323E-10	1.3726E-10	10.42	1.5383E-10	1.3766E-10	10.51	1.6837E-10	1.4938E-10	11.28
Tl	81	202.972344	3.1901E-10	2.8637E-10	10.23	3.2865E-10	2.9465E-10	10.35	3.2995E-10	2.9552E-10	10.43	3.2182E-10	2.8578E-10	11.20
		204.974428	7.6901E-10	6.9003E-10	10.27	7.9226E-10	7.0994E-10	10.39	7.9538E-10	7.1204E-10	10.48	7.7579E-10	6.8855E-10	11.25
Pb	82	203.973044	3.5774E-10	3.2125E-10	10.20	3.6855E-10	3.3053E-10	10.32	3.7000E-10	3.3151E-10	10.40	3.7729E-10	3.3517E-10	11.17
		205.974465	3.5604E-09	3.1957E-09	10.24	3.6680E-09	3.2880E-09	10.36	3.6824E-09	3.2978E-09	10.45	3.6014E-09	3.1976E-09	11.21
		206.975897	3.8584E-09	3.4624E-09	10.26	3.9750E-09	3.5623E-09	10.38	3.9906E-09	3.5729E-09	10.47	3.9772E-09	3.5304E-09	11.23
		207.976652	1.0964E-08	9.8364E-09	10.28	1.1295E-08	1.0120E-08	10.40	1.1339E-08	1.0150E-08	10.49	1.1392E-08	1.0110E-08	11.26
Bi	83	208.980399	8.6357E-10	7.7504E-10	10.25	8.6943E-10	7.7925E-10	10.37	8.7285E-10	7.8158E-10	10.46	8.3197E-10	7.3859E-10	11.22
Th	90	232.038055	2.2478E-10	1.5858E-10	29.45	2.3157E-10	1.6309E-10	29.57	2.3248E-10	1.6358E-10	29.64	2.3745E-10	1.6541E-10	30.34
U	92	235.043930	4.4124E-13	0.0000E+00	100.00	4.3412E-13	0.0000E+00	100.00	4.3583E-13	0.0000E+00	100.00	4.5550E-13	0.0000E+00	100.00
		238.050788	6.1617E-11	2.5751E-11	58.21	6.0623E-11	2.5275E-11	58.31	6.0861E-11	2.5345E-11	58.36	6.3608E-11	2.6131E-11	58.92
Z	–	–	*2.1663E-02*	*1.9509E-02*	*–9.95*	*1.9940E-02*	*1.7934E-02*	*–10.06*	*1.8810E-02*	*1.6905E-02*	*–10.13*	*1.4783E-02*	*1.3181E-02*	*–10.83*

Table 4. For each adopted solar distribution, the initial (x_{in}) and the present-day ($x_{\odot}$) mass fractions and the corresponding values of the P and R parameters.

El.	AG89				GN93				GS98				Lo03			
	x_{in}	$x_{\odot}$	P	R	x_{in}	$x_{\odot}$	P	R	x_{in}	$x_{\odot}$	P	R	x_{in}	$x_{\odot}$	P	R
H	0.6973	0.7310	0.862	1.616	0.7018	0.7354	0.861	1.616	0.7038	0.7376	0.861	1.627	0.7127	0.7479	0.853	1.611
He	0.2810	0.2495	1.018	1.544	0.2783	0.2466	1.018	1.544	0.2774	0.2455	1.019	1.553	0.2726	0.2389	1.021	1.532
Li	1.1419E-08	3.7929E-09	2.750	1.112	1.1496E-08	4.1896E-09	2.503	1.153	1.1541E-08	4.4981E-09	2.339	1.193	1.0999E-08	5.6412E-09	1.764	1.295
Be	1.9100E-10	1.6900E-10	1.021	1.543	1.9229E-10	1.6988E-10	1.022	1.542	1.9305E-10	1.7038E-10	1.022	1.552	1.9268E-10	1.6847E-10	1.023	1.531
B	6.6079E-09	5.8904E-09	1.014	1.546	5.4075E-09	4.8133E-09	1.014	1.545	5.4287E-09	4.8275E-09	1.014	1.555	5.4188E-09	4.7753E-09	1.015	1.535
C	3.5138E-03	3.1554E-03	1.006	1.549	3.4571E-03	3.1004E-03	1.006	1.549	3.2390E-03	2.9023E-03	1.006	1.559	2.4524E-03	2.1791E-03	1.007	1.538
N	1.2663E-03	1.1387E-03	1.005	1.550	1.0604E-03	9.5235E-04	1.005	1.549	9.4879E-04	8.5134E-04	1.005	1.559	7.8766E-04	7.0101E-04	1.005	1.539
O	1.0972E-02	9.8790E-03	1.004	1.550	9.6212E-03	8.6518E-03	1.004	1.550	8.8091E-03	7.9148E-03	1.004	1.560	6.5179E-03	5.8090E-03	1.004	1.540
F	4.6229E-07	4.1538E-07	1.006	1.549	5.5956E-07	5.0213E-07	1.006	1.549	4.6725E-07	4.1893E-07	1.006	1.559	4.5574E-07	4.0525E-07	1.006	1.539
Ne	1.9956E-03	1.7992E-03	1.002	1.551	1.9634E-03	1.7679E-03	1.002	1.550	1.9711E-03	1.7734E-03	1.002	1.561	1.2413E-03	1.1080E-03	1.003	1.540
Na	3.7821E-05	3.4056E-05	1.004	1.550	3.9871E-05	3.5857E-05	1.004	1.550	3.9117E-05	3.5149E-05	1.004	1.560	3.8154E-05	3.4008E-05	1.004	1.540
Mg	7.4454E-04	6.7185E-04	1.001	1.551	7.4959E-04	6.7559E-04	1.001	1.551	7.5254E-04	6.7768E-04	1.001	1.561	7.3401E-04	6.5583E-04	1.002	1.541
Al	6.5654E-05	5.9207E-05	1.002	1.551	6.4594E-05	5.8181E-05	1.002	1.551	6.7904E-05	6.1111E-05	1.002	1.561	6.4725E-05	5.7790E-05	1.002	1.540
Si	8.0293E-04	7.2553E-04	1.000	1.552	8.0837E-04	7.2959E-04	1.000	1.551	8.3045E-04	7.4891E-04	1.000	1.562	8.1000E-04	7.2484E-04	1.000	1.541
P	9.2723E-06	8.3710E-06	1.001	1.551	7.0814E-06	6.3854E-06	1.001	1.551	9.1585E-06	8.2515E-06	1.001	1.561	6.9342E-06	6.1989E-06	1.001	1.541
S	4.8108E-04	4.3503E-04	0.999	1.552	4.2184E-04	3.8101E-04	0.999	1.552	4.1386E-04	3.7350E-04	0.999	1.562	4.1307E-04	3.6994E-04	0.999	1.542
Cl	5.3192E-06	4.8030E-06	1.001	1.551	9.0945E-06	8.2021E-06	1.001	1.551	5.5015E-06	4.9576E-06	1.001	1.561	5.3660E-06	4.7979E-06	1.001	1.541
Ar	1.0614E-04	9.6011E-05	0.999	1.552	9.7460E-05	8.8053E-05	0.999	1.552	7.4222E-05	6.7004E-05	0.999	1.562	1.0706E-04	9.5911E-05	0.999	1.542
K	4.2496E-06	3.8412E-06	1.000	1.552	4.1810E-06	3.7747E-06	1.000	1.552	4.2953E-06	3.8747E-06	1.000	1.562	4.0009E-06	3.5815E-06	1.000	1.541
Ca	7.0648E-05	6.3953E-05	0.998	1.552	7.4479E-05	6.7342E-05	0.998	1.552	7.3070E-05	6.6016E-05	0.998	1.562	6.9648E-05	6.2448E-05	0.998	1.542
Sc	4.4564E-08	4.0234E-08	1.001	1.551	5.3940E-08	4.8641E-08	1.001	1.551	4.6091E-08	4.1528E-08	1.001	1.561	4.3933E-08	3.9274E-08	1.001	1.541
Ti	3.2835E-06	2.9628E-06	1.001	1.551	4.0669E-06	3.6653E-06	1.001	1.551	3.3960E-06	3.0581E-06	1.001	1.561	3.3116E-06	2.9586E-06	1.002	1.541
V	4.2980E-07	3.8760E-07	1.002	1.551	4.1324E-07	3.7220E-07	1.002	1.551	4.3441E-07	3.9095E-07	1.002	1.561	4.2372E-07	3.7829E-07	1.002	1.540
Cr	2.0052E-05	1.8104E-05	1.001	1.551	1.9729E-05	1.7790E-05	1.001	1.551	2.0740E-05	1.8686E-05	1.001	1.561	1.9769E-05	1.7672E-05	1.001	1.541
Mn	1.4999E-05	1.3535E-05	1.001	1.551	1.0940E-05	9.8598E-06	1.001	1.551	1.5160E-05	1.3653E-05	1.001	1.561	1.4450E-05	1.2911E-05	1.002	1.541
Fe	1.4561E-03	1.3155E-03	1.000	1.552	1.4326E-03	1.2927E-03	1.000	1.551	1.4382E-03	1.2967E-03	1.000	1.561	1.4028E-03	1.2549E-03	1.000	1.541
Co	3.8597E-06	3.4850E-06	1.001	1.551	3.9764E-06	3.5859E-06	1.001	1.551	3.9011E-06	3.5152E-06	1.001	1.561	3.8051E-06	3.4017E-06	1.001	1.541
Ni	8.4090E-05	7.6061E-05	0.999	1.552	8.4659E-05	7.6487E-05	0.999	1.552	8.4992E-05	7.6724E-05	0.999	1.562	8.1020E-05	7.2577E-05	0.999	1.542
Cu	9.5341E-07	8.6087E-07	1.001	1.551	8.3601E-07	7.5395E-07	1.001	1.551	1.0091E-06	9.0926E-07	1.001	1.561	9.6181E-07	8.5987E-07	1.001	1.541
Zn	2.3537E-06	2.1258E-06	1.000	1.551	2.1119E-06	1.9052E-06	1.000	1.551	2.4910E-06	2.2453E-06	1.000	1.561	2.3744E-06	2.1234E-06	1.001	1.541
Ga	7.5783E-08	6.8361E-08	1.002	1.551	7.6296E-08	6.8739E-08	1.002	1.551	7.6596E-08	6.8952E-08	1.002	1.561	7.3010E-08	6.5200E-08	1.002	1.540
Ge	2.4965E-07	2.2512E-07	1.002	1.551	2.5134E-07	2.2636E-07	1.002	1.551	2.5233E-07	2.2706E-07	1.002	1.561	2.5170E-07	2.2470E-07	1.002	1.540
As	1.4151E-08	1.2762E-08	1.002	1.551	1.4247E-08	1.2833E-08	1.002	1.551	1.4303E-08	1.2872E-08	1.002	1.561	1.3020E-08	1.1624E-08	1.002	1.540
Se	1.4451E-07	1.3019E-07	1.003	1.550	1.6704E-07	1.5030E-07	1.003	1.550	1.6770E-07	1.5076E-07	1.003	1.560	1.5266E-07	1.3614E-07	1.003	1.540
Br	2.7808E-08	2.5075E-08	1.002	1.551	2.7996E-08	2.5213E-08	1.002	1.550	2.8106E-08	2.5291E-08	1.002	1.561	2.6180E-08	2.3369E-08	1.003	1.540
Kr	1.1471E-07	1.0335E-07	1.003	1.550	1.3884E-07	1.2493E-07	1.003	1.550	1.3939E-07	1.2532E-07	1.003	1.560	1.3283E-07	1.1845E-07	1.003	1.540
Rb	1.7298E-08	1.5291E-08	1.022	1.542	1.7821E-08	1.5733E-08	1.022	1.542	1.7891E-08	1.5782E-08	1.022	1.552	1.6286E-08	1.4249E-08	1.022	1.532
Sr	6.0086E-08	5.4165E-08	1.002	1.551	5.9116E-08	5.3222E-08	1.003	1.550	5.9349E-08	5.3387E-08	1.003	1.560	5.9235E-08	5.2855E-08	1.003	1.540
Y	1.1888E-08	1.0723E-08	1.002	1.551	1.2248E-08	1.1033E-08	1.002	1.551	1.2296E-08	1.1067E-08	1.002	1.561	1.1720E-08	1.0464E-08	1.002	1.540
Zr	2.9943E-08	2.7007E-08	1.002	1.551	3.0146E-08	2.7156E-08	1.002	1.551	3.0265E-08	2.7240E-08	1.002	1.561	3.0207E-08	2.6970E-08	1.002	1.540
Nb	1.8804E-09	1.6965E-09	1.002	1.551	1.8931E-09	1.7059E-09	1.002	1.551	1.9005E-09	1.7111E-09	1.002	1.561	2.0326E-09	1.8154E-09	1.002	1.540
Mo	7.0494E-09	6.3579E-09	1.002	1.551	7.2625E-09	6.5419E-09	1.002	1.551	7.2911E-09	6.5621E-09	1.002	1.561	7.7977E-09	6.9618E-09	1.002	1.540
Ru	5.3804E-09	4.8516E-09	1.002	1.551	5.5430E-09	4.9920E-09	1.002	1.551	5.5648E-09	5.0074E-09	1.002	1.561	5.3040E-09	4.7343E-09	1.003	1.540
Rh	1.0201E-09	9.2002E-10	1.002	1.551	1.0509E-09	9.4667E-10	1.002	1.551	1.0550E-09	9.4957E-10	1.002	1.561	1.0776E-09	9.6207E-10	1.002	1.540
Pd	4.3192E-09	3.8937E-09	1.002	1.551	4.3485E-09	3.9151E-09	1.002	1.550	4.3656E-09	3.9271E-09	1.002	1.560	4.4588E-09	3.9786E-09	1.003	1.540

Table 4. continued.

El.	AG89				GN93				GS98				Lo03			
	x_{in}	$x_{\odot}$	P	R	x_{in}	$x_{\odot}$	P	R	x_{in}	$x_{\odot}$	P	R	x_{in}	$x_{\odot}$	P	R
Ag	1.5104E-09	1.3620E-09	1.002	1.551	1.5206E-09	1.3696E-09	1.002	1.551	1.5266E-09	1.3738E-09	1.002	1.561	1.5237E-09	1.3601E-09	1.002	1.540
Cd	5.2120E-09	4.6960E-09	1.003	1.550	5.2473E-09	4.7218E-09	1.003	1.550	5.2680E-09	4.7363E-09	1.003	1.560	5.1382E-09	4.5821E-09	1.003	1.540
In	6.1123E-10	5.5071E-10	1.003	1.550	6.1537E-10	5.5374E-10	1.003	1.550	6.1779E-10	5.5543E-10	1.003	1.560	6.0258E-10	5.3735E-10	1.003	1.540
Sn	1.3203E-08	1.1889E-08	1.003	1.550	1.3293E-08	1.1954E-08	1.004	1.550	1.3345E-08	1.1991E-08	1.004	1.560	1.2720E-08	1.1336E-08	1.004	1.539
Sb	1.0757E-09	9.6838E-10	1.004	1.550	1.0583E-09	9.5151E-10	1.004	1.550	1.0625E-09	9.5441E-10	1.004	1.560	1.1628E-09	1.0360E-09	1.004	1.539
Te	1.7866E-08	1.6064E-08	1.005	1.549	1.7987E-08	1.6151E-08	1.005	1.549	1.8058E-08	1.6200E-08	1.005	1.559	1.7612E-08	1.5668E-08	1.006	1.539
I	3.3088E-09	2.9783E-09	1.004	1.550	3.3312E-09	2.9946E-09	1.004	1.550	3.3443E-09	3.0037E-09	1.004	1.560	3.6600E-09	3.2602E-09	1.005	1.539
Xe	1.7951E-08	1.6147E-08	1.005	1.550	1.5741E-08	1.4140E-08	1.005	1.549	1.5803E-08	1.4183E-08	1.005	1.559	2.0317E-08	1.8084E-08	1.005	1.539
Cs	1.4117E-09	1.2701E-09	1.004	1.550	1.4544E-09	1.3068E-09	1.004	1.550	1.4601E-09	1.3108E-09	1.005	1.560	1.3917E-09	1.2391E-09	1.005	1.539
Ba	1.7945E-08	1.6135E-08	1.005	1.549	1.8488E-08	1.6600E-08	1.005	1.549	1.8560E-08	1.6651E-08	1.005	1.559	1.7691E-08	1.5739E-08	1.006	1.539
La	1.7738E-09	1.5953E-09	1.005	1.550	1.8700E-09	1.6796E-09	1.005	1.549	1.8774E-09	1.6846E-09	1.005	1.559	1.7487E-09	1.5561E-09	1.006	1.539
Ce	4.5992E-09	4.1378E-09	1.004	1.550	4.8485E-09	4.3566E-09	1.004	1.550	4.8676E-09	4.3696E-09	1.005	1.560	4.7478E-09	4.2268E-09	1.005	1.539
Pr	6.8411E-10	6.1578E-10	1.004	1.550	7.2121E-10	6.4836E-10	1.004	1.550	7.2405E-10	6.5030E-10	1.004	1.560	7.0622E-10	6.2907E-10	1.005	1.539
Nd	3.4299E-09	3.0863E-09	1.004	1.550	3.6159E-09	3.2496E-09	1.004	1.550	3.6301E-09	3.2593E-09	1.004	1.560	3.4601E-09	3.0810E-09	1.005	1.539
Sm	1.1306E-09	1.0123E-09	1.009	1.548	1.1648E-09	1.0416E-09	1.009	1.547	1.1694E-09	1.0447E-09	1.010	1.557	1.1147E-09	9.8751E-10	1.010	1.537
Eu	4.2456E-10	3.8194E-10	1.004	1.550	4.3739E-10	3.9300E-10	1.004	1.550	4.3911E-10	3.9416E-10	1.005	1.560	4.1855E-10	3.7260E-10	1.005	1.539
Gd	1.4886E-09	1.3381E-09	1.005	1.549	1.5694E-09	1.4088E-09	1.005	1.549	1.5755E-09	1.4130E-09	1.006	1.559	1.5018E-09	1.3356E-09	1.006	1.539
Tb	2.7377E-10	2.4613E-10	1.005	1.549	2.8862E-10	2.5915E-10	1.005	1.549	2.8975E-10	2.5991E-10	1.005	1.559	2.6990E-10	2.4009E-10	1.006	1.539
Dy	1.8495E-09	1.6622E-09	1.005	1.549	1.9498E-09	1.7501E-09	1.006	1.549	1.9575E-09	1.7553E-09	1.006	1.559	1.8233E-09	1.6213E-09	1.006	1.539
Ho	4.2024E-10	3.7768E-10	1.005	1.549	4.3294E-10	3.8860E-10	1.006	1.549	4.3464E-10	3.8974E-10	1.006	1.559	4.2394E-10	3.7696E-10	1.006	1.539
Er	1.2011E-09	1.0794E-09	1.005	1.549	1.2662E-09	1.1365E-09	1.006	1.549	1.2712E-09	1.1399E-09	1.006	1.559	1.2399E-09	1.1025E-09	1.006	1.539
Tm	1.8362E-10	1.6505E-10	1.005	1.549	1.9357E-10	1.7378E-10	1.005	1.549	1.9433E-10	1.7429E-10	1.006	1.559	1.8102E-10	1.6099E-10	1.006	1.539
Yb	1.2426E-09	1.1165E-09	1.006	1.549	1.2802E-09	1.1488E-09	1.006	1.549	1.2852E-09	1.1521E-09	1.006	1.559	1.2536E-09	1.1143E-09	1.007	1.538
Lu	1.8584E-10	1.6663E-10	1.008	1.548	1.9146E-10	1.7145E-10	1.008	1.548	1.9221E-10	1.7195E-10	1.008	1.558	1.7904E-10	1.5882E-10	1.009	1.537
Hf	7.7232E-10	6.9378E-10	1.006	1.549	8.1420E-10	7.3048E-10	1.006	1.549	8.1740E-10	7.3261E-10	1.006	1.559	8.7419E-10	7.7690E-10	1.007	1.538
Ta	1.9667E-10	1.7667E-10	1.006	1.549	1.0881E-10	9.7622E-11	1.006	1.549	1.0924E-10	9.7907E-11	1.006	1.559	1.0903E-10	9.6897E-11	1.007	1.538
W	7.0901E-10	6.3682E-10	1.006	1.549	7.3045E-10	6.5524E-10	1.006	1.549	7.3332E-10	6.5715E-10	1.006	1.559	6.8304E-10	6.0692E-10	1.007	1.538
Re	2.7938E-10	2.3923E-10	1.055	1.528	2.8782E-10	2.4615E-10	1.055	1.528	2.8895E-10	2.4686E-10	1.055	1.538	2.8184E-10	2.3869E-10	1.056	1.517
Os	3.6769E-09	3.3012E-09	1.006	1.549	3.7881E-09	3.3967E-09	1.007	1.549	3.8030E-09	3.4066E-09	1.007	1.559	3.7093E-09	3.2945E-09	1.008	1.538
Ir	3.6306E-09	3.2600E-09	1.006	1.549	3.6552E-09	3.2779E-09	1.006	1.549	3.6696E-09	3.2875E-09	1.007	1.559	3.5793E-09	3.1793E-09	1.007	1.538
Pt	7.5144E-09	6.7466E-09	1.006	1.549	7.7416E-09	6.9416E-09	1.007	1.549	7.7720E-09	6.9619E-09	1.007	1.559	7.5895E-09	6.7406E-09	1.008	1.538
Au	1.0730E-09	9.6345E-10	1.006	1.549	1.1311E-09	1.0144E-09	1.006	1.549	1.1356E-09	1.0174E-09	1.007	1.559	1.1076E-09	9.8389E-10	1.007	1.538
Hg	1.9885E-09	1.7850E-09	1.007	1.549	2.1951E-09	1.9679E-09	1.007	1.549	2.2037E-09	1.9737E-09	1.007	1.559	2.4118E-09	2.1416E-09	1.008	1.538
Tl	1.0880E-09	9.7641E-10	1.007	1.549	1.1209E-09	1.0046E-09	1.007	1.548	1.1253E-09	1.0076E-09	1.007	1.558	1.0976E-09	9.7433E-10	1.008	1.538
Pb	1.8740E-08	1.6816E-08	1.007	1.549	1.9306E-08	1.7301E-08	1.007	1.548	1.9382E-08	1.7352E-08	1.007	1.558	1.9348E-08	1.7173E-08	1.008	1.538
Bi	8.6357E-10	7.7504E-10	1.007	1.549	8.6943E-10	7.7925E-10	1.007	1.548	8.7285E-10	7.8158E-10	1.007	1.558	8.3197E-10	7.3859E-10	1.008	1.538
Th	2.2478E-10	1.5858E-10	1.281	1.444	2.3157E-10	1.6309E-10	1.282	1.444	2.3248E-10	1.6358E-10	1.282	1.454	2.3745E-10	1.6541E-10	1.285	1.433
U	6.2058E-11	2.5751E-11	2.178	1.214	6.1057E-11	2.5275E-11	2.180	1.213	6.1297E-11	2.5345E-11	2.181	1.223	6.4063E-11	2.6131E-11	2.194	1.200